

# On a three-dimensional and two four-dimensional oncolytic viro-therapy models

Rim Adenane<sup>a</sup>, Eric Avila-Vales<sup>b</sup>, Florin Avram<sup>c</sup>,  
Andrei Halanay<sup>d</sup>, Angel G. C. Pérez<sup>b</sup>

October 4, 2022

<sup>a</sup> Département des Mathématiques, Université Ibn-Tofail, Kenitra, 14000, Maroc

<sup>b</sup> Facultad de Matemáticas, Universidad Autónoma de Yucatán, Anillo Periférico Norte,  
Tablaje Catastral 13615, C.P. 97119, Mérida, Yucatán, Mexico

<sup>c</sup> Laboratoire de Mathématiques Appliquées, Université de Pau, 64000, Pau, France

<sup>d</sup> Department of Mathematics and Informatics, Polytechnic University of Bucharest,  
062203, Bucharest, Romania

## Abstract

We revisit here and carry out further works on tumor-virotherapy compartmental models of [Tian, 2011, Wang et al., 2013, Phan and Tian, 2017, Guo et al., 2019]. The results of these papers are only slightly pushed further. However, what is new is the fact that we make public our electronic notebooks, since we believe that easy electronic reproducibility is crucial in an era in which the role of the software becomes very important.

**Keywords:** Oncolytic viro-therapy, immune response, stability, compartmental models, bifurcation analysis, electronic reproducibility.

## Contents

1	Introduction	2
2	Warm-up: the 3 dimensional viral model [Tian, 2011, Kim et al., 2020]	7

<b>3</b>	<b>The four-compartment viro-therapy and immunity model (1)</b>	<b>12</b>
3.1	Boundedness . . . . .	12
3.2	Boundary equilibria and their stability . . . . .	14
3.2.1	Stability of the boundary fixed point $E_K$ . . . . .	15
3.2.2	Stability of the boundary fixed point $E_*$ . . . . .	16
<b>4</b>	<b>The four-dimensional viro-therapy model with <math>\epsilon = 0</math> [Phan and Tian, 2017]</b>	<b>17</b>
4.1	Interior equilibria . . . . .	17
4.2	The stability of $E_*$ when $\epsilon = 0$ . . . . .	19
4.3	Stability of the interior equilibria and bifurcation diagrams . . . . .	19
4.4	Time and phase plots illustrating bi-stability and a limit cycle, with $\epsilon = 0$ . . . . .	24
4.4.1	Bi-stability in the interval $(b_2, b_{2*})$ . . . . .	24
4.4.2	Limit cycle in the interval $(b_H, b_\infty)$ . . . . .	25
<b>5</b>	<b>The four-dimensional viro-therapy model of [Guo et al., 2019], with logistic growth</b>	<b>26</b>
5.1	Interior equilibria . . . . .	26
5.2	Stability of interior equilibria and bifurcation diagrams . . . . .	29
5.3	Time and phase plots illustrating different behaviors, with $\epsilon = 1$ . . . .	32
5.3.1	Stability of $E_+$ in the interval $(b_0, b_H)$ . . . . .	32
5.3.2	Bi-stability and limit cycle in the interval $(b_H, b_{2*})$ . . . . .	34
5.3.3	Chaotic behavior in the interval $(b_{2*}, b_\infty)$ . . . . .	34
<b>6</b>	<b>Conclusions</b>	<b>35</b>

# 1 Introduction

**Compartmental models** became famous first in mathematical epidemiology, following the pioneering work of Kermack and McKendrick [Kermack and McKendrick, 1927] on the SIR model; see [Haddad et al., 2010] for other domains of application, and for some general theory. In the last thirty years, they have penetrated also in mathematical virology [Perelson and Weisbuch, 1997, Nowak and May, 2000, Wodarz and Komarova, 2005, Bocharov et al., 2018], and in mathematical oncolytic virotherapy, i.e. in the modeling of the use of viruses for treating tumors [Santiago et al., 2017, Rockne et al., 2019, Pooladvand, 2021].

We may distinguish between at least two main directions of work in these fields.

1. Part of the literature is dedicated to creating models to fit specific viruses and therapies – see for example [Perelson and Nelson, 1999, Perelson, 2002, Antonio Chiocca, 2002, Smith and De Leenheer, 2003, Wodarz, 2003, Pillis et al., 2006, Dalal et al., 2008, Tuckwell and Wan, 2000, Yuan and Allen, 2011, Yu and Wei, 2009, Huang et al., 2011, Chenar et al., 2018]. The models proposed are high dimensional, and hence only analyzable numerically, for particular instances of the parameters.
2. Another part, which is our concern here, is in applying sophisticated mathematical tools, notably the theory of bifurcations for dynamical systems, to “lower dimensional caricatures” of more complex models. This requires the use of both symbolic software like Mathematica, Maple, or Sagemath, and also of sophisticated numeric continuation and bifurcation packages like MatCont (written in Matlab), PyDSTool (Python), XPPAuto (C) – see [Blyth et al., 2020] for a recent review, and BifurcationsKit (written in Julia).

In our work below, we have combined the use of MatCont – see [Pérez, 2022] with that of Mathematica – see [Adenane, 2022], and in particular the package EcoEvo. The notebooks offered on GitHub are an important part of our work, and we attempted to achieve a roughly one to one correspondence between the equations numbered in the text and those displayed in Mathematica.

The origins of the glioma viro-therapy four-compartment  $(x, y, v, z)$  model considered here, where untreated and tumor cells are denoted respectively by  $x, y$ , virus cells by  $v$ , and innate immune cell by  $z$ , are in [O’Connell et al., 1999, Friedman et al., 2006].<sup>¶</sup> Interestingly, these papers suggested a density dependent rate of immune cells, linear up to a threshold  $z_0$ , and quadratic afterwards. “The first process occurs when  $z$  is small and yields a linear clearance; the second process occurs when  $z$  is large and yields a quadratic clearance” [Friedman et al., 2006, pg 2]. Subsequent papers of Tian [Phan and Tian, 2017], [Guo et al., 2019] tackled symbolically the two particular cases  $z_0 = \infty$ ,  $z_0 = 0$ . For further developments and further outstanding questions in the field, see [Vithanage et al., 2021, Phan and Tian, 2022a, Phan and Tian, 2022b].

Since the quadraticity is hard to ascertain, we propose to study a unification of

---

<sup>¶</sup>A four-dimensional model considerably more complex was proposed in [Senekal et al., 2021].

the four-compartment systems studied in [Phan and Tian, 2017, Guo et al., 2019]:

$$\begin{aligned}
\frac{dx}{dt} &= \lambda x \left(1 - \frac{x+y}{K}\right) - \beta xv \\
\frac{dy}{dt} &= \beta xv - \gamma y - \beta_y yz \\
\frac{dv}{dt} &= b\gamma y - \beta xv - \delta v - \beta_v vz \\
\frac{dz}{dt} &= z(\rho\beta_y y - cz^\epsilon), \quad \epsilon \in \{0, 1\},
\end{aligned} \tag{1}$$

where  $x$ ,  $y$ ,  $v$  and  $z$  represent the populations of uninfected (untreated) tumor cell population, infected tumor cell population, free virus and innate immune cells, respectively.

**Remark 1.1.** *The invariance of the first quadrant (also called “essential non-negativity”) is immediate since each component  $f_i(X)$  of the dynamics may be decomposed as*

$$f_i(X) = g_i(X) - x_i h_i(X),$$

where  $g_i, h_i$  are polynomials with nonnegative coefficients, and  $x_i$  is the variable whose rate is given by  $f_i(X)$ . In fact, under this absence of “negative cross-effects”, even more is true: the model admits a “mass-action representation” by the so-called “Hungarian lemma” [Hárs and Tóth, 1981, Haddad et al., 2010], [Tóth et al., 2018, Thm. 6.27] <sup>§</sup>

**Remark 1.2.** *Scaling all the variables by  $x = K\tilde{x}$ ,  $y = K\tilde{y}$ , ... has the effect of multiplying all the quadratic terms by  $K$ , and one may finally assume  $K = 1$ , at the price of renaming some other parameters. Also, scaling time by a constant allows choosing another parameter as 1. Below, we will follow occasionally [Tian, 2011, Phan and Tian, 2017] in choosing  $K = \gamma = 1$ , which simplifies a bit the results.*

Figure 1 depicts a schematic diagram of this model. The interpretation of parameters can be seen in Table 1.

---

<sup>§</sup>The previous virology literature does not seem to be aware of this result, and offers direct proofs instead.

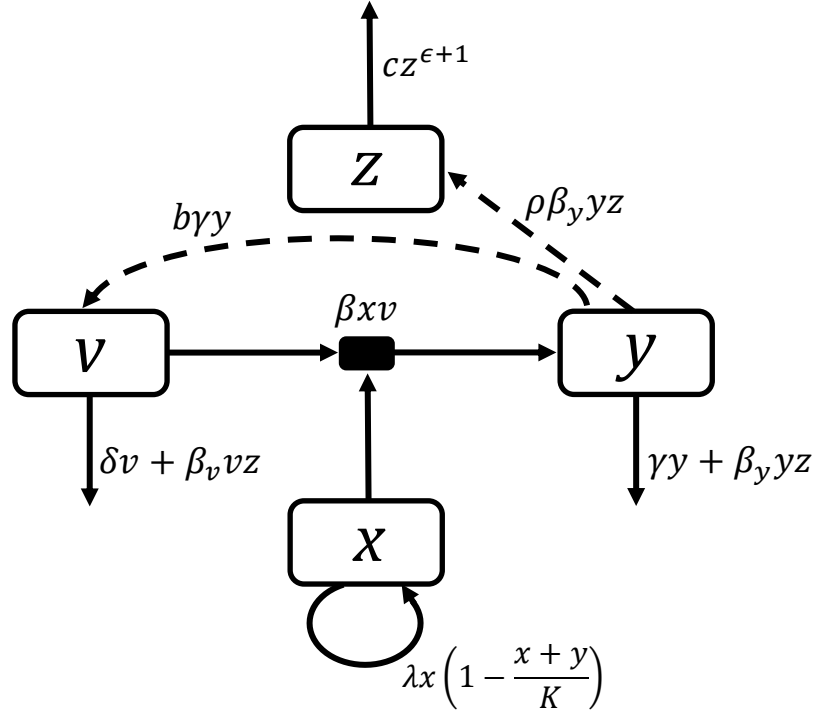


Figure 1: Schematic diagram of model (1). The compartments  $x$ ,  $y$ ,  $v$  and  $z$  denote uninfected tumor cells, infected tumor cells, free virus and innate immune cells, respectively. Continuous lines represent transfer between compartments. Dashed lines represent viral production or activation of immune cells.

Table 1: Interpretation of parameters for model (1).

Symbol	Description
$\lambda$	intrinsic growth rate of uninfected tumor cells
$K > 0$	carrying capacity of uninfected tumor cells
$\beta > 0$	viral infection rate
$\beta_y$	rate at which immune system removes infected tumor cells
$\gamma > 0$	lysis rate of infected cells
$b \geq 1$	virus burst size
$\delta$	clearance rate of viruses
$\beta_v$	rate at which immune system removes viruses
$\rho\beta_y := \beta_z > 0$	proliferation rate of immune cells due to the interaction with infected tumor cells
$c$	rate of clearance of immune cells

**Remark 1.3.** When  $\beta_y = \beta_v = 0$  (the immune system is totally inefficient), the general model (1) reduces to a three-compartment viral model (2) of [Tian, 2011, Kim et al., 2020].

The fourth compartment for the immune system was subsequently modeled differently in [Phan and Tian, 2017] and in [Guo et al., 2019] (where  $K = \infty$ ). We have unified these two papers by adding the parameter  $\epsilon$ , which equals 0 in [Phan and Tian, 2017] and 1 in [Guo et al., 2019].

The [Tian, 2011] three compartment model has been analyzed symbolically up to a point, and it ended with a list of open problems, which awoke our attention, since they seemed to be still open. Other interesting open problems were raised by the two four-compartment model (for example, the local stability of certain points was only established in particular cases, numerically).

We point out now another important open problem, not mentioned in [Tian, 2011].

**Q:** Can chaos arise in model (1)?

Note that while we do have the right to hope for the absence of complicated dynamical behaviors, since we are dealing with a pseudo-linear, essentially non-negative system, this is by no means guaranteed. Indeed, complicated dynamics like multiple “concentric” cycles have been found in [Ruan and Wang, 2003], and in the parallel ecology literature on **three dimensional food-chains**, chaos is known to occur as well [Klebanoff and Hastings, 1994, Kuznetsov and Rinaldi, 1996, Kuznetsov et al., 2001, Deng, 2001, Deng and Hines, 2003, Deng, 2004, Deng, 2006, Deng et al., 2017].

While very interesting and worthy of further investigation, the virology papers cited above suffer from the lack of providing supporting electronic notebooks. The importance of symbolic and numeric computing in mathematical biology cannot be overstated (see for example [Brown et al., 2006]).

**Electronic reproducibility.** As emphasized already 30 years ago, the opportunity we have nowadays of being able to accompany our pencil calculations with electronic notebooks “gives a new meaning to reproducible research” [Claerbout and Karrenbach, 1992]. Following efforts of numerous people, for example [Buckheit and Donoho, 1995, Donoho, 2010], lots of progress has been achieved, as witnessed by the existence of the platform GitHub. Unfortunately, the percentage of researchers who take the time to tidy their notebooks and make them available on GitHub is still infinitesimal in some fields.

Our main contribution below is in providing electronic notebooks, where the readers may recover the results of the previous works of [Tian, 2011, Wang et al., 2013, Phan and Tian, 2017, Guo et al., 2019], and then modify them as they please,

for analyzing similar models. Note this is a non-trivial task, and it goes in a direction orthogonal to that of most of the current literature.

**Contents.** We start by revisiting in Section 2 the three-dimensional model of [Tian, 2011], which had been already essentially solved symbolically. However, with help from Mathematica, we resolve one of the problems left open in [Tian, 2011].

In Section 3 we introduce a “generalized virus” model, geared at unifying previous studies and initiating new directions of research (as typical in the field, we will not be able to answer all our questions).

Some first results for our general model are then presented in Sections 3.1, 3.2.

The particular case of [Phan and Tian, 2017] is revisited in Section 4.

We turn then to the complete viro-therapy and immunity model with logistic growth in Section 5.

## 2 Warm-up: the 3 dimensional viral model [Tian, 2011, Kim et al., 2020]

The three-dimensional tumor-virus model proposed in [Tian, 2011, (5)], [Wang et al., 2013] is:

$$\begin{aligned}\frac{dx}{dt} &= \lambda x \left(1 - \frac{x+y}{K}\right) - \beta xv \\ \frac{dy}{dt} &= \beta xv - \gamma y \\ \frac{dv}{dt} &= b\gamma y - \beta xv - \delta v, \quad x+y \leq K, \quad v \leq \frac{b\gamma K}{\delta}.\end{aligned}\tag{2}$$

**Brief history.** A similar three-dimensional  $(x, y, v)$  model, with linear growth, and with the term  $\beta xv$  present in all the equations seems to have been first proposed by Anderson, May and Gupta [Anderson et al., 1989], as a model for the interaction of parasites with host-cells, in particular red blood cells (RBC). Subsequently, this became known as the Novak-May model [Nowak and May, 2000], and has been applied in many other directions, for example by Tuckwell & Wan [Tuckwell and Wan, 2000], as a model for HIV-1 dynamics. See also [Tian, 2011], [Wang et al., 2013] for a version with delay, [Phan and Tian, 2020] for a stochastic version, , and see [Camara et al., 2022] for a stochastic version with “saturated infection rate” in which  $\beta$  is replaced by  $\beta(x, y) = \frac{\beta}{x+y+\alpha}$ .

Factorization yields easily the three equilibrium points for the model (2). The

first two  $E_0 = (0, 0, 0)$ ,  $E_K = (K, 0, 0)$  are “infection free”, and the third equilibrium

$$E_* = \left( \frac{\delta}{\beta(b-1)}, \lambda \frac{\delta}{\beta(b-1)} \frac{K\beta(b-1) - \delta}{K\beta\gamma(b-1) + \lambda\delta}, \lambda \frac{\gamma}{\beta} \frac{K\beta(b-1) - \delta}{K\beta\gamma(b-1) + \lambda\delta} \right)$$

is interior to the domain.

The explicit eigenvalues of the Jacobian at the first equilibrium point make it a saddle point. Similarly, examining the Jacobian shows that the second point is stable when

$$R_0 := \frac{\beta K}{\beta K + \delta} b \quad (3)$$

is smaller than 1 and unstable when  $R_0 > 1$ , where  $R_0$  is the famous “basic reproduction number”. Note however that the results of [Van den Driessche and Watmough, 2002, Van den Driessche and Watmough, 2008] do not apply here due to the existence of two “disease free” equilibria.

The critical  $b$  which makes  $R_0 = 1$  is

$$b_0 = 1 + \frac{\delta}{\beta K}, \quad (4)$$

confirming Lemma [Tian, 2011, Lem. 3.4]. Writing the third point as

$$E_* = \left( \frac{\delta}{\beta(b-1)}, \frac{\delta\lambda}{\beta(b-1)} \frac{\beta K + \delta}{K\beta\gamma(b-1) + \lambda\delta} (R_0 - 1), \frac{\gamma\lambda}{\beta} \frac{\beta K + \delta}{K\beta\gamma(b-1) + \lambda\delta} (R_0 - 1) \right).$$

It is convenient to rescale time by  $\gamma$  and the variables by  $K$ , the net result being that these variables may be assumed to equal 1 [Tian, 2011, Sec. 3.1]. The third point simplifies then to

$$E_* = \left( \frac{\delta}{\beta(b-1)}, \frac{\delta\lambda}{\beta(b-1)} \frac{\beta + \delta}{\beta(b-1) + \lambda\delta} (R_0 - 1), \frac{\lambda}{\beta} \frac{\beta + \delta}{\beta(b-1) + \lambda\delta} (R_0 - 1) \right) \quad (5)$$

and we see that this point enters the nonnegative domain precisely when  $R_0 = 1$ , at  $E_* = E_*(b_0) = E_K = (1, 0, 0)$ .

$E_*$  interior to the invariant domain iff  $R_0 > 1$ . Its stability may be tackled via the Routh-Hurwitz conditions, which, at order three, amounts to  $\begin{cases} \text{Tr}(J) < 0, \\ \text{Tr}(J)M_2(J) < \text{Det}(J) < 0, \end{cases}$  where  $M_2$  is the sum of the second-order principal leading minors of the Jacobian matrix  $J$  at  $E_*$ . Now the first and last inequalities are always satisfied in our case



[Tian, 2011, Thm. 3.7] since,  $\begin{cases} Tr(J) := -1 + \frac{\delta(b\beta+\lambda)}{\beta(1-b)} < 0 \\ Det(J) := (1 - R_0) \left( \frac{\delta\lambda(\beta+\delta)}{\beta(b-1)} \right) < 0 \end{cases}$ , and thus the local stability of the point  $E_*$  holds iff

$$H(b) := Det(J) - Tr(J)M_2(J) = -a_3 + a_1a_2 > 0, \quad (6)$$

where

$$\begin{aligned} a_1 &:= \frac{\beta(b + b\delta - 1) + \delta\lambda}{(b-1)\beta}, \\ a_2 &:= \frac{\delta\lambda((b-1)\beta(\beta-1+\delta+b(1-\beta+\delta)) + ((b-1)^2\beta + b\delta^2)\lambda)}{(b-1)^2\beta((b-1)\beta + \delta\lambda)}, \\ a_3 &:= \delta\lambda \left( 1 + \frac{\delta}{\beta(1-b)} \right). \end{aligned}$$

**Remark 2.1.** As a check, note that  $H(b_0) = \lambda(1 + \delta + \beta)(1 + \delta + \lambda + \beta) > 0$ , and so  $E_*$  is stable at the critical point when  $E_K$  loses its stability, as expected.

To analyze the sign of  $H(b)$ , we note first that its denominator  $(b-1)^3\beta^2((b-1)\beta + \delta\lambda)$  is always positive (see second cell in notebook [Mathematica, 2022a]).

Positivity reduces thus to the positivity of the numerator, which is a fourth order polynomial

$$\Phi(b) = B_4b^4 + B_3b^3 + B_2b^2 + B_1b + B_0, \quad (7)$$

and may be investigated via Descartes's rule.

The coefficients are

$$\begin{cases} B_4 := -\beta^3, \\ B_3 := \beta^2(-\beta(\delta-3) + \delta(\delta+3) + \lambda+1), \\ B_2 := \beta(\beta^2(2\delta-3) - 3\beta(2\delta+\lambda+1) + \delta\lambda(\delta(\delta+3) + \lambda+1)), \\ B_1 := -\beta^3(\delta-1) + \beta^2(-\delta^2 + 3\delta + 3\lambda + 3) - \beta\delta\lambda(3\delta + 2\lambda + 2) + \delta^3\lambda^2, \\ B_0 := \beta(\lambda+1)(\delta\lambda - \beta). \end{cases}$$

By using  $B_4 < 0$ ,  $\Phi(b_0) = \frac{\delta^3(1+\lambda)(1+\beta+\delta)(1+\beta+\delta+\lambda)}{\beta} > 0$ , [Tian, 2011, Lem. 3.8] concludes that the fourth order polynomial  $\Phi(b)$  must have at least one root larger than  $b_0$ , and one root smaller than  $b_0$ . Letting  $b_H$  denote the smaller root larger than  $b_0$ , [Tian, 2011, Thm 3.9] concludes that local stability holds in  $(b_0, b_H)$ . Also,  $b_H$  is a candidate for a Hopf bifurcation, by the following elementary Lemma.

**Lemma 2.1.** [Tian, 2011, Lem. 3.10] *A cubic polynomial  $\lambda^3 + a_1\lambda^2 + a_2\lambda + a_3$  with real coefficients has a pair of pure imaginary roots if and only if  $a_2 > 0$  and  $a_3 = a_1a_2$ . When it has pure imaginary roots, these are given by  $\pm i\sqrt{a_2}$ , the real root is given by  $-a_1$ , and  $a_1a_3 > 0$ .*

**Remark 2.2.** *Higher dimension extensions exist as well – see [Farkas and Simon, 1992, Guckenheimer et al., 1997].*

[Tian, 2011] conjectured that  $E_*$  may regain its stability at still larger values of  $b$ , after crossing yet larger roots, and the question of whether this may occur: “What conditions can guarantee that the function  $H(b)$  has four, three, and two distinct real zeros?”

The precise classification of polynomials by their number of roots is a complicated problem [Prodanov, 2021], and we do not address it below. We may answer however the stability question, using the observation in the next remark.

**Remark 2.3.** *The real roots smaller than  $b_0$  have no importance (for stability), so the real question is whether the fourth-order polynomial  $\Phi(b)$  given by (7) may have more than one real root larger than  $b_0$ .*

*This can be tackled by shifting the polynomial to  $\Phi(b_0 + x)$  and applying Descartes upper bound on the maximum number of positive roots via the number of sign changes in the sequence of coefficients of the shifted polynomial.*

**Lemma 2.2.** *The polynomial  $\Phi(b)$  defined in (7) has precisely one real root  $b_H$  larger than  $b_0$ .*

*Proof.* The coefficients of the shifted polynomial  $\Phi(b_0 + x)$  are

$$\begin{cases} \tilde{B}_0 := \frac{\delta^3(\lambda+1)(\beta+\delta+1)(\beta+\delta+\lambda+1)}{\beta}, \\ \tilde{B}_1 := \delta^2(\beta(2\delta\lambda + 3\delta + 3\lambda + 3) + (\delta + 2)\lambda^2 + 2\delta(\delta + 3)\lambda + \delta(3\delta + 5) + 5\lambda + 3), \\ \tilde{B}_2 := \beta\delta(-\beta^2 + \delta(\delta + 3)\lambda + 3\delta(\delta + 1) + \lambda^2 + 4\lambda + 3), \\ \tilde{B}_3 := \beta^2(-\beta(\delta + 1) + (\delta - 1)\delta + \lambda + 1), \\ \tilde{B}_4 := -\beta^3. \end{cases}$$

The first two are positive and the last negative, so in order to have three roots larger than  $b_0$  it is necessary that the third coefficient is negative and the fourth positive. Now each of this inequalities admits solutions, but the command

$$\text{Reduce}[\{\text{cofi}[[4]] > 0 \& \& \text{cofi}[[3]] < 0\}]$$

at the end of the second cell in the Mathematica file [Mathematica, 2022a] yields False, telling us that the system of the two inequalities doesn't. Similarly,

$$\text{FindInstance}[\{cofi[[4]] > 0 \& \& cofi[[3]] < 0\}, par]$$

fails. The diligent reader is invited to provide a “human proof”, but warned that this seems hard.  $\square$

A bifurcation diagram of model (2) as  $b$  varies is illustrated in Figure 2.

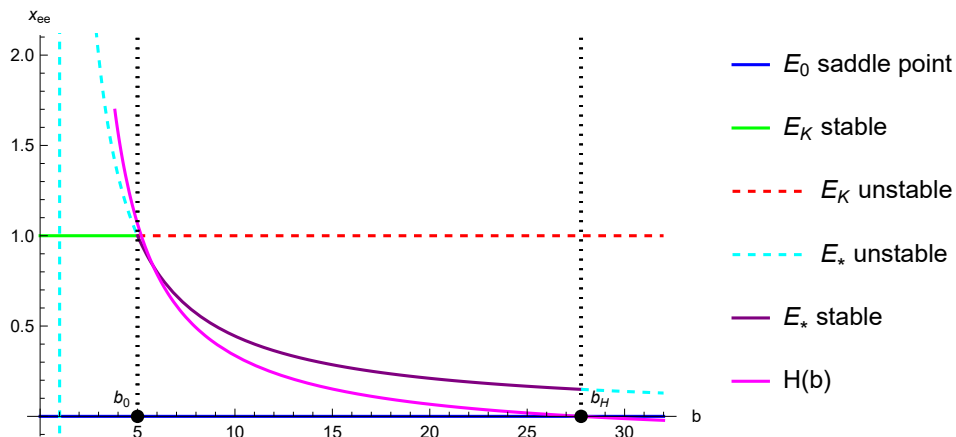
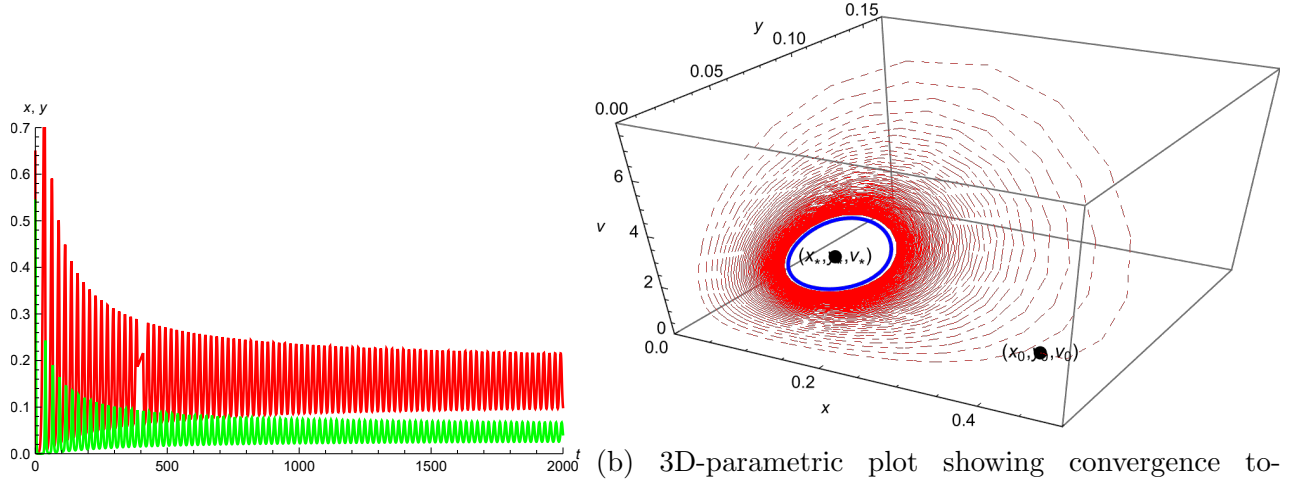


Figure 2: Bifurcation diagram when  $b$  varies, when  $\lambda = 0.36$ ,  $\beta = 0.11$ ,  $\delta = 0.44$ ,  $K = \gamma = 1 \implies b_0 = 1 + \frac{\delta}{\beta} = 5$ ,  $b_H = 27.7664$ . When  $b$  is bigger than the Hopf bifurcation point  $b_H$ , there are no stable fix points.

Figures 3a and 3b show an illustration of the cycle arising with the parameter set above, at a value  $b = 28$  slightly larger than  $b_H$ , see also [Wang et al., 2013, Figure 7].



(a)  $(x, y)$ -time plot suggests the existence of periodicity.

(b) 3D-parametric plot showing convergence towards an attracting cycle. Two paths are displayed, one starting near the unstable fixed point  $E_* = (0.148148, 0.0431317, 2.64672)$ , with eigenvalues  $\{-1.51022, 0.000296187 \pm 0.298909Im\}$ , and one starting far away.

Figure 3: Time and 3D parametric plot when  $b = 28 > b_H = 27.7664$ .

### 3 The four-compartment viro-therapy and immunity model (1)

#### 3.1 Boundedness

**Theorem 3.1.** *The epidemiological domain*

$$\Omega = \left\{ (x, y, v, z) \in \mathbb{R}_+^4; x(t) + y(t) \leq K, v(t) \leq \frac{b\gamma K}{\delta}, z(t) \leq \zeta \right\},$$

where

$$\zeta = \begin{cases} \frac{\rho\beta b\gamma K^2}{\delta \min\{\gamma, c\}}, & \text{if } \epsilon = 0; \\ \frac{\rho\beta_y K}{c}, & \text{if } \epsilon = 1. \end{cases}$$

is a positively invariant set.

**Remark 3.1.** *The first conditions on  $x, y, v$  appear already in [Phan and Tian, 2017, Lem. 1].*

*Proof.* By adding the first two equations in (1), one obtains

$$\begin{aligned}\dot{x} + \dot{y} &= \lambda x \left(1 - \frac{x+y}{K}\right) - \beta xv + \beta xv - \beta_y yz - \gamma y \\ &\leq \lambda x \left(1 - \frac{x+y}{K}\right).\end{aligned}$$

By a comparison argument we obtain that  $\limsup_{t \rightarrow \infty} x(t) + y(t) \leq K$ . This implies that for all  $\varepsilon > 0$  there is  $t_1 > 0$  such that if  $t > t_1$  then  $x(t) \leq K + \varepsilon$  and  $y(t) \leq K + \varepsilon$ . Then, for  $t > t_1$  we have

$$\dot{v} = b\gamma y - \beta xv - \delta v - \beta_v zv \leq b\gamma(K + \varepsilon) - \delta v,$$

from which we deduce that  $\limsup_{t \rightarrow \infty} v(t) \leq \frac{b\gamma K}{\delta}$ .

Lastly, for the boundedness of  $z$ , we will divide the proof in two cases. Let  $\varepsilon_2 > 0$  and take  $t_2 > 0$  such that

$$x(t) + y(t) \leq K + \varepsilon_2 \quad \text{and} \quad v(t) \leq \frac{b\gamma K}{\delta} + \varepsilon_2 \quad \text{for } t > t_2.$$

Consider first the case  $\epsilon = 0$ . Let  $w(t) = y(t) + \frac{1}{\rho}z(t)$ . Then, for  $t > t_2$ , we have

$$\begin{aligned}\dot{w} &= \dot{y} + \frac{1}{\rho}\dot{z} \\ &= \beta xv - \gamma y - \frac{c\beta_y}{\beta_z}z \\ &\leq \beta(K + \varepsilon_2) \left( \frac{b\gamma K}{\delta} + \varepsilon_2 \right) - \sigma \left( y + \frac{1}{\rho}z \right),\end{aligned}$$

where  $\sigma := \min\{\gamma, c\}$ . It follows that

$$\limsup_{t \rightarrow \infty} \frac{1}{\rho}z(t) \leq \limsup_{t \rightarrow \infty} w(t) \leq \frac{\beta b\gamma K^2}{\delta\sigma},$$

and finally

$$\limsup_{t \rightarrow \infty} z(t) \leq \frac{s\beta b\gamma K^2}{\beta_y \delta \min\{\gamma, c\}}.$$

Lastly, in the case when  $\epsilon = 1$ , we obtain

$$\begin{aligned}\dot{z} &= \beta_z yz - cz^2 \\ &\leq \beta_z(K + \varepsilon_2)z - cz^2 \\ &= \beta_z(K + \varepsilon_2)z \left(1 - \frac{c}{\beta_z(K + \varepsilon_2)}z\right)\end{aligned}$$

for  $t > t_2$ . From this, we deduce that  $\limsup_{t \rightarrow \infty} z(t) \leq \frac{\beta_z K}{c}$ . □

### 3.2 Boundary equilibria and their stability

Factoring the last and first equilibrium equations yields four points which have either  $z = 0$  or  $x = 0$ :

**Theorem 3.2.** *The fixed points with  $z = 0$  or  $x = 0$  are respectively:*

- $E_0 = (0, 0, 0, 0)$
- $E_K = (K, 0, 0, 0)$
- $E_* = \left( \frac{\delta}{\beta(b-1)}, y_* := \frac{\delta}{\beta(b-1)} \frac{b\lambda(R_0 - 1)}{\lambda(b - R_0) + (b-1)\gamma R_0}, \frac{\gamma(b-1)}{\delta} y_*, 0 \right)$ . (8)
- $E_N = \left( 0, y_e = \frac{c}{s}, -y_e \frac{b\gamma\mu_y}{\gamma\mu_v - \delta\mu_y}, -\frac{\gamma}{\mu_y} \right)$  when  $\epsilon = 0$  and  $(0, -y_e \frac{\gamma}{\mu}, y_e \frac{\gamma^2 b}{\gamma\beta_v - \delta\mu}, -\frac{\gamma}{\beta_y})$  when  $\epsilon = 1$ . This is always outside the domain and will be ignored from now on.

**Remark 3.2.** *The first three fixed points appear already as solutions of the three-dimensional system [Tian, 2011, (5)] obtained when the immune system is inexistent.*

*Indeed, with  $K = 1$ ,  $\gamma = 1$  (after rescaling), as in section [Tian, 2011, Sec. 3.1], the second and third point become  $(1, 0, 0)$  and  $\left( \frac{\delta}{\beta(b-1)}, \lambda \frac{\delta}{\beta(b-1)} \frac{\beta(b-1) - \delta}{\beta(b-1) + \lambda\delta}, \frac{\gamma\lambda}{\beta} \frac{\beta(b-1) - \delta}{\beta(b-1) + \lambda\delta} \right)$  –see [Tian, 2011, Sec. 3.2].*

*The fourth fixed point appeared also already, in the linear growth problem of [Guo et al., 2019].*

The Jacobian matrix of the system when  $K = \gamma = 1$  is given by

$$J(x, y, v, z) = \begin{pmatrix} \lambda - \frac{\lambda(2x+y)}{K} - \beta v & -\frac{\lambda x}{K} & -\beta x & 0 \\ \beta v & -\gamma - z\mu_y & \beta x & -y\mu_y \\ -\beta v & b\gamma & -\delta - z\mu_v + \beta(-x) & -v\mu_v \\ 0 & sz & 0 & sy - c(\epsilon + 1)z^\epsilon \end{pmatrix}.$$

At the boundary fixed points, the Jacobian has a block-diagonal form, which simplifies the stability analysis.

**Theorem 3.3.**  *$E_0$  is always a saddle point.*

*Proof.* Since

$$J(E_0) = \begin{pmatrix} \lambda & 0 & 0 & 0 \\ 0 & -\gamma & 0 & 0 \\ 0 & b\gamma & -\delta & 0 \\ 0 & 0 & 0 & c_e \end{pmatrix},$$

where  $c_e = c(-0^\epsilon)(\epsilon+1) = \begin{cases} -c & \epsilon = 0 \\ 0 & \epsilon = 1 \end{cases}$ , it has always one positive eigenvalue  $\lambda > 0$ , and at least two negative eigenvalues  $-\gamma, -\delta$ .  $\square$

### 3.2.1 Stability of the boundary fixed point $E_K$

Here we will prove the existence of a stability transition of  $E_K$  when  $R_0 = 1$ , in the spirit of the “ $R_0$  alternative”. The proof is standard when  $\epsilon = 0$  <sup>§</sup>, but the result is more delicate when  $\epsilon = 1$ , since the Jacobian is singular at  $E_K$ :

$$\begin{pmatrix} -\lambda & -\lambda & -\beta & 0 \\ 0 & -z\mu_y - 1 & \beta & 0 \\ 0 & b & -\beta - \delta - z\mu_v & 0 \\ 0 & sz & 0 & -c(\epsilon+1)z^\epsilon \end{pmatrix}$$

**Theorem 3.4.** *When  $\epsilon = 1$ ,  $E_K = (K, 0, 0, 0)$  is*

1. *unstable if  $R_0 > 1 \Leftrightarrow b > b_0$ ;*
2. *stable if  $R_0 < 1, \epsilon = 0$ ;*
3. *when  $R_0 < 1, \epsilon = 0$ , the equilibrium  $E_K$  is locally stable and local asymptotic stability holds with respect to  $(x, y, v)$ , i.e. every solution that starts close enough to  $E_K$  satisfies  $\lim_{t \rightarrow \infty} (x, y, v)(t) = (K, 0, 0)$ .*

*Proof.* The Jacobian at  $E_K$  is

$$J(E_K) = \begin{pmatrix} -\lambda & -\lambda & -K\beta & 0 \\ 0 & -\gamma & \beta K & 0 \\ 0 & b\gamma & -K\beta - \delta & 0 \\ 0 & 0 & 0 & 0 \end{pmatrix}.$$

---

<sup>§</sup>and global stability holds as well under the assumptions  $R_0 < 1$  and  $y_e > 1$  [Phan and Tian, 2017, Prop. 4]

The block diagonal structure puts in evidence an upper  $1 \times 1$  block with negative eigenvalue  $-\lambda$ , and a lower  $1 \times 1$  block with eigenvalue equal to 0. The remaining middle  $2 \times 2$  diagonal block has determinant  $\gamma(\beta K + \delta)(1 - R_0)$ , implying eigenvalues of different sign when  $R_0 > 1$ , yielding the first part of the result.

The trace is always negative, implying two negative eigenvalues from the middle block when  $R_0 < 1$ . Together with the last eigenvalue  $-c$ , this yields the second result.

When  $R_0 < 1, \epsilon = 1$ , our system is in the delicate situation covered by the Lyapunov-Malkin Theorem (since the fixed point is never hyperbolic and the Hartman-Grobman Theorem does not apply), [Malkin, 1959, Ch. IV, §34], [Zenkov et al., 2002]. Even if one condition of this theorem is not fulfilled for the shifted vector  $(x_1 = x - K, y, v, z)$ , namely  $f_4(0, 0, 0, z) = -cz^2$  is not zero for every  $z$  as required, the proof still yields simple local stability due to the specific form of  $f_4(x_1, y, v, z) = z(sy - cz^2)$ . The asymptotic behavior of  $z$  cannot be inferred using the original proof any more.  $\square$

### 3.2.2 Stability of the boundary fixed point $E_*$

At  $E_*$ , the Jacobian has a block-tridiagonal form:

**Theorem 3.5.** *If  $R_0 = \frac{\beta K}{\beta K + \delta} b > 1$  (same value as in the three-dimensional model),  $E_*$  is non-negative, and an unstable equilibrium point.*

*Proof.* The Jacobian is given by

$$J(E_*) = \begin{pmatrix} a_1 & a_2 & a_3 & 0 \\ a_4 & a_5 & a_6 & a_7 \\ -a_4 & b\gamma & a_8 & a_9 \\ 0 & 0 & 0 & c_e + \rho\beta_y y_* \end{pmatrix}, \quad (9)$$

where  $c_e = \begin{cases} -c & \epsilon = 0 \\ 0 & \epsilon = 1 \end{cases}$ , where  $y_* = \frac{\delta}{\beta(b-1)} \frac{b\lambda(R_0-1)}{\lambda(b-R_0)+(b-1)\gamma R_0}$  is the  $y$  coordinate of the fixed point  $E_*$  (8), and where  $a_1, a_2, a_3, a_4, a_5, a_6, a_7, a_8$  and  $a_9$  have complicated expressions, given in the first cell in [Mathematica, 2022b].

When  $\epsilon = 1$ , using  $b > 1$  and  $1 < R_0 < b$  implies that  $J(E_*)$  has at least one positive eigenvalue and therefore is unstable.



When  $\epsilon = 0$ , we still get a sufficient condition for instability

$$y_* > y_e = \frac{c}{\rho\beta_y}, \quad (10)$$

but this condition is not necessary, since a second instability interval (due to the other three eigenvalues) may appear – see Figure 4. The full analysis is reported to section 4.2. □

The interior equilibria of system (1) will be studied in the following sections for two special cases of the model. From now on, we will use mainly the rescaled equations with  $K = \gamma = 1$ .

## 4 The four-dimensional viro-therapy model with $\epsilon = 0$ [Phan and Tian, 2017]

The dynamical system when  $K = \gamma = 1$  and  $\epsilon = 0$ , is:

$$\begin{aligned} \frac{dx}{dt} &= \lambda x (1 - x - y) - \beta x v \\ \frac{dy}{dt} &= \beta x v - \beta_y y z - y \\ \frac{dv}{dt} &= b y - \beta x v - \beta_v v z - \delta v \\ \frac{dz}{dt} &= z(\beta_z y - c), \end{aligned} \quad (11)$$

with

$$y \leq 1 - x, \quad v \leq \min \left[ \frac{\lambda}{\beta}(1 - y_e), \frac{y_e}{\delta}(b - 1) \right], \quad y_e = \frac{c}{\beta_z}. \quad (12)$$

Besides the three equilibrium points  $E_0, E_K, E_*$  of the three-dimensional viral system (extended by the values  $z = 0$ ), we may have up to two new equilibria with  $z > 0$ , both having  $y = y_e$ , provided that  $y_e \leq 1$  –see below.

### 4.1 Interior equilibria

When  $z \neq 0$ , from the last equation in (11) we have  $y = y_e = \frac{c}{\beta_z}$ , and by substitution into the first equation of (11), we get

$$x = 1 - y_e - \frac{v\beta}{\lambda} =: h(v).$$

If  $y_e > 1$ , there are no equilibrium points with  $z > 0$ . When  $y_e \leq 1$ , then  $x$  positive requires  $v \leq \frac{\lambda}{\beta}(1 - y_e)$

Moreover, substituting this into the sum of the second and third equations in (11) yields

$$z = \frac{y_e(b-1) - v\delta}{y_e\beta_y + v\beta_v} =: \frac{f(v)}{g(v)},$$

which is positive if and only if  $v \leq \frac{c(b-1)}{\beta_z\delta}$ , and the second equilibrium equation in (11) implies

$$P(v) = v\beta h(v) - y_e \left( 1 + \beta_y \frac{f(v)}{g(v)} \right) := v^3 + a_2v^2 + a_1v + a_0 = 0,$$

$$\begin{cases} a_2 := y_e(1 + \frac{\lambda}{\beta}) - \frac{\lambda}{\beta} = b_0y_e - b_0 + 1, \\ a_1 := \frac{\lambda}{\beta^2}y_e \left[ 1 + \frac{\beta\mu_y}{\beta_v}(y_e - b_0) \right], \\ a_0 := \frac{bc^2\lambda\mu_y}{\beta^2\beta_z^2\beta_v}. \end{cases}$$

This third order equation determining  $v$  may have at most two sign changes, attained when  $y_e \leq \max[(b_0 - 1)/b_0, b_0 - \frac{\beta_v}{\beta\beta_y}]$ , and so we may have either 0, 1 or 2 positive endemic equilibria, denoted by  $E_{im}, E_+$ ; there may also be a solution  $E_-$  with negative  $v$ , which is of no concern to us. All situations may occur –see the bifurcation diagram in Figure 4, depending on the sign of the discriminant of  $P(b)$ , which will be denoted by  $Dis$ .

Note that

$$Dis(b) = 0 \Leftrightarrow b = (b_{1*}, b_{2*}) = \mp \frac{1}{27\beta^2c^2\lambda\beta_z^2\beta_v^2\beta_y^2} \times$$

$$\left[ 2\sqrt{\beta^2\beta_z^2\beta_y^2 (\beta^2c^2\beta_y^2 + \lambda\beta_v^2 (\lambda(c - \beta_z)^2 - 3c\beta_z) + c\lambda\beta_v\beta_y(\beta_z(\beta + 3\delta) - \beta c))}^3 \right.$$

$$- \beta\beta_z\beta_y (\lambda(c - \beta_z)\beta_v + \beta c\beta_y) \times$$

$$\left. (2\beta^2c^2\beta_y^2 + \lambda\beta_v^2 (2\lambda(c - \beta_z)^2 - 9c\beta_z) + c\lambda\beta_v\beta_y(-5\beta c + 5\beta\beta_z + 9\delta\beta_z)) \right]$$

**Remark 4.1.** *Biologically, the equilibrium  $E_0$  a boundary case in which the model is inappropriate. The equilibrium  $E_K$  occurs when viro-therapy fails, and the tumor cell density reaches its carrying capacity in the long run. Lastly,  $E_*$  represents a partial success of viro-therapy where healthy and infected tumor cells coexist, and which may be achieved by viruses only, without help from the immune system.*

Finally,  $E_{im}$  represents another possible coexistence, which requires help from the immune system, and  $E_{\pm}$  represent equilibria which are exterior to the domain or unstable.

## 4.2 The stability of $E_*$ when $\epsilon = 0$

As already hinted by (10), the stability of  $E_*$  is affected by the value of  $y_e$ .

**Lemma 4.1.** *[Phan and Tian, 2017, Prop. 6,7]  $E^*$  is locally stable if and only if  $b \in (b_0, b_H) \cap (b_1, b_2)^c$ , where  $(b_1, b_2)$  is the interval on which  $y_*(b) > y_e$ .*

We provide now a proof reducing the problem to three dimensions which is considerably shorter than the original.

**Proof:** This result follows from the block diagonal structure of the Jacobian at  $E^*$ , see (9), which yields one eigenvalue proportional to  $y_* - y_e$ , and must of course be negative for local stability. Under this condition, stability is thus equivalent to that of the remaining three-dimensional block, which is identical to that in [Tian, 2011] (unfortunately, that is not immediately obvious, due to different notations).

The new condition  $p(b) = y_*(b)/y_e = \frac{\delta\lambda\beta_z(\beta+\delta)(1-R_0)}{(b-1)\beta c((b-1)\beta+\delta\lambda)} < 1$  may be explicitized with respect to  $b$  into  $b \notin (b_1, b_2)$ ,

$$b_{1,2} = \frac{2\beta c - c\delta\lambda \mp \delta\sqrt{\lambda}\sqrt{\lambda(c - \beta_z)^2 - 4c\beta_z} + \delta\lambda\beta_z}{2\beta c} \quad (13)$$

In conclusion, the stability domain is the intersection of that in [Tian, 2011] with  $b \notin (b_1, b_2)$ .  $\square$

## 4.3 Stability of the interior equilibria and bifurcation diagrams

We illustrate now the results of [Phan and Tian, 2017, Prop 6-8] via bifurcation diagrams of  $v$  and  $x$  with respect to  $b$  in a particular numeric case.

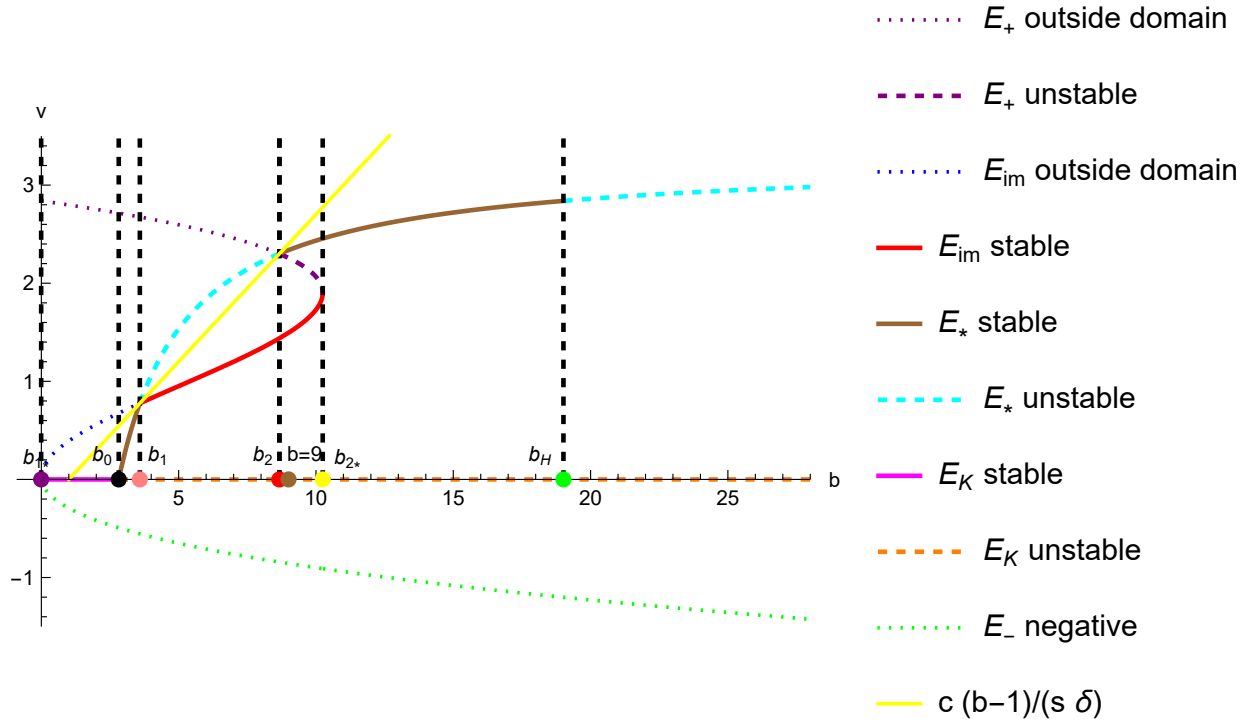


Figure 4: Bifurcation diagram of system (11) when  $K = \gamma = 1$ ,  $\epsilon = 0$ , and  $\beta_v = 0.16$ ,  $\beta_y = 0.48$ ,  $\lambda = 0.36$ ,  $\beta = 0.11$ ,  $\delta = 0.2$ ,  $\beta_z = 0.6$ ,  $c = 0.036$ , which yields  $y_e = 0.06$ ,  $b_0 = 2.81818$ ,  $b_H = 19.01210747136$ , and  $Dis = 0 \Leftrightarrow b_{1*} = -0.00697038$ , and  $b_{2*} = 10.2462$ . The values of  $b_1, b_2$  are 3.58676, 8.66779. Note that at these two values,  $E_*$  equals  $E_{im}$  and  $E_+$ , respectively, and that these points are at the yellow boundary of the domain of admissible values for  $v$ .

Since the variable of interest is  $x$ , we provide also a bifurcation diagram of  $x$  with respect to  $b$ .

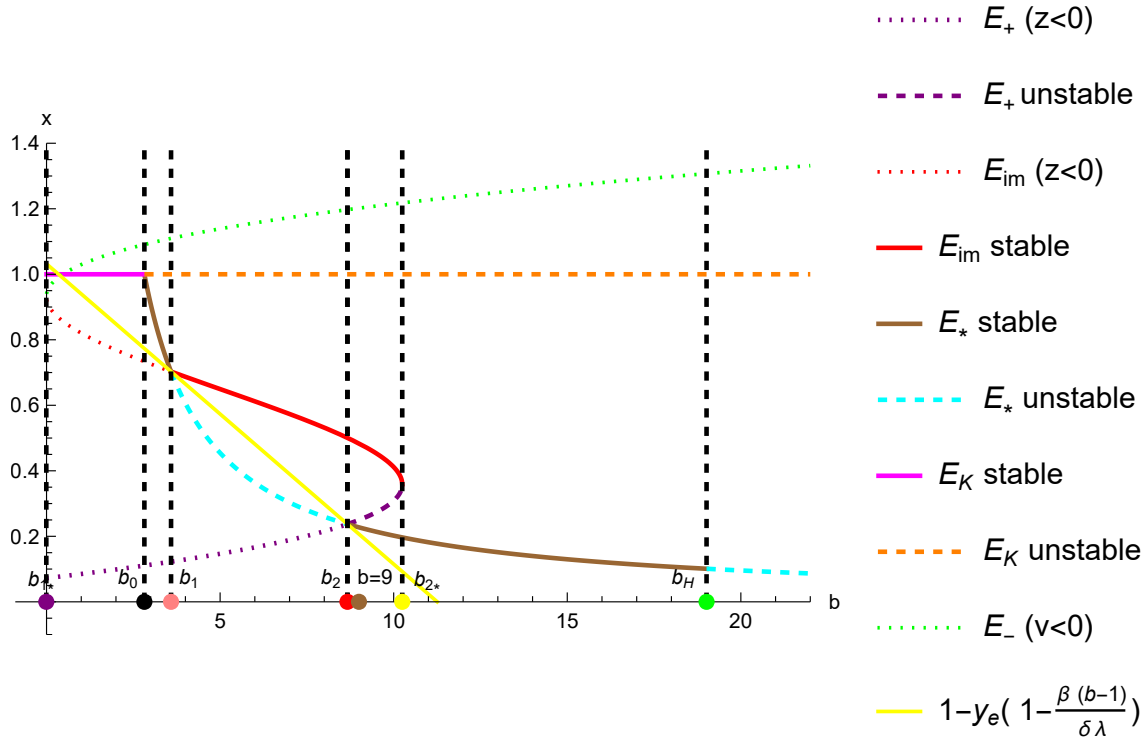


Figure 5: Bifurcation diagram of system (11), representing the  $x$  of the equilibria points, as functions of  $b$ . The last curve corresponds to the constraint  $v \geq 0$ . The parameters are  $K = \gamma = 1$ ,  $\epsilon = 0$ , and  $\beta_v = 0.16$ ,  $\beta_y = 0.48$ ,  $\lambda = 0.36$ ,  $\beta = 0.11$ ,  $\delta = 0.2$ ,  $\beta_z = 0.6$ ,  $c = 0.036$ .

**Remark 4.2.** *Note that:*

1. For a “weak virus” with  $b < b_0$ ,  $E_K$  is the only stable equilibrium, as expected from the fact that  $E_K$  behaves essentially as the disease free equilibrium from mathematical epidemiology.
2. At the first critical point  $b = b_0$  which corresponds to  $R_0$ , the “stability relay” is passed from  $E_K$  to the “virus only” equilibrium  $E_*$ , precisely when this enters the domain.
3. As the virus becomes more efficient,  $E_*$  becomes unstable, precisely at the point  $b = b_1$  when the fixed point  $E_{im}$  which involves the immunity system enters the domain. This point carries the “stability relay” until  $b_2$ .

4. *As the efficiency of the virus increases to  $b = b_2$ ,  $E_*$  becomes stable again and we have bistability, until  $b_{2*}$ . In this range, reaching a better outcome  $E_*$  or a worse one  $E_{im}$  depends on the boundary conditions, until  $b_{2*}$ .*
5. *After  $b_{2*}$ ,  $E_{im}$  becomes unfeasible, and  $E_*$  remains the only stable equilibrium, until  $b_H$ .*
6. *After  $b_H$ ,  $E_*$  loses again its stability, in favor of a limit cycle.*

Let us discuss now the stability of the interior equilibrium points, via the so-called Routh-Hurwitz-Lienard-Chipart-Schur-Cohn-Jury (RH) criteria [Anderson and Jury, 1973, Wiggers and Pedersen, 2018, Daud, 2021], which are formulated in terms of the coefficients of the characteristic polynomial  $Det(\lambda I_n - L) = \lambda^n + a_1 \lambda^{n-1} + \dots + a_n$ , and of certain Hurwitz determinants  $H_i$  [Wiggers and Pedersen, 2018, (15.22)].

In the fourth order case, the characteristic polynomial is  $Det(J - zI_4) = z^4 + a_3 z^3 + a_2 z^2 + a_1 z + a_0 = z^4 - Tr(J)z^3 + z^2 M_2(J) - z M_3(J) + Det(J)$ , where  $M_2, M_3$  are the sums of the second and third order principal leading minors of the Jacobian  $J$ , respectively. The Routh-Hurwitz becomes [Wiggers and Pedersen, 2018, pg. 137]

$$\begin{cases} Tr(J) < 0, & M_2 > 0, & M_3 < 0, & Det(J) > 0, \\ 0 < Tr(J) (M_2 M_3 - Tr(J) Det(J)) - M_3^2. \end{cases}$$

Pinpointing the domains of attraction associated with the two equilibrium points  $E_*, E_{im}$  symbolically is quite challenging, but feasible in particular cuts see Figures 6 and 7. Note that in this case our analysis may help with controlling the evolution of treatment, by privileging the desired final tumor size.

Figure 6 depicts a bifurcation diagram with respect to  $b, \beta$ .

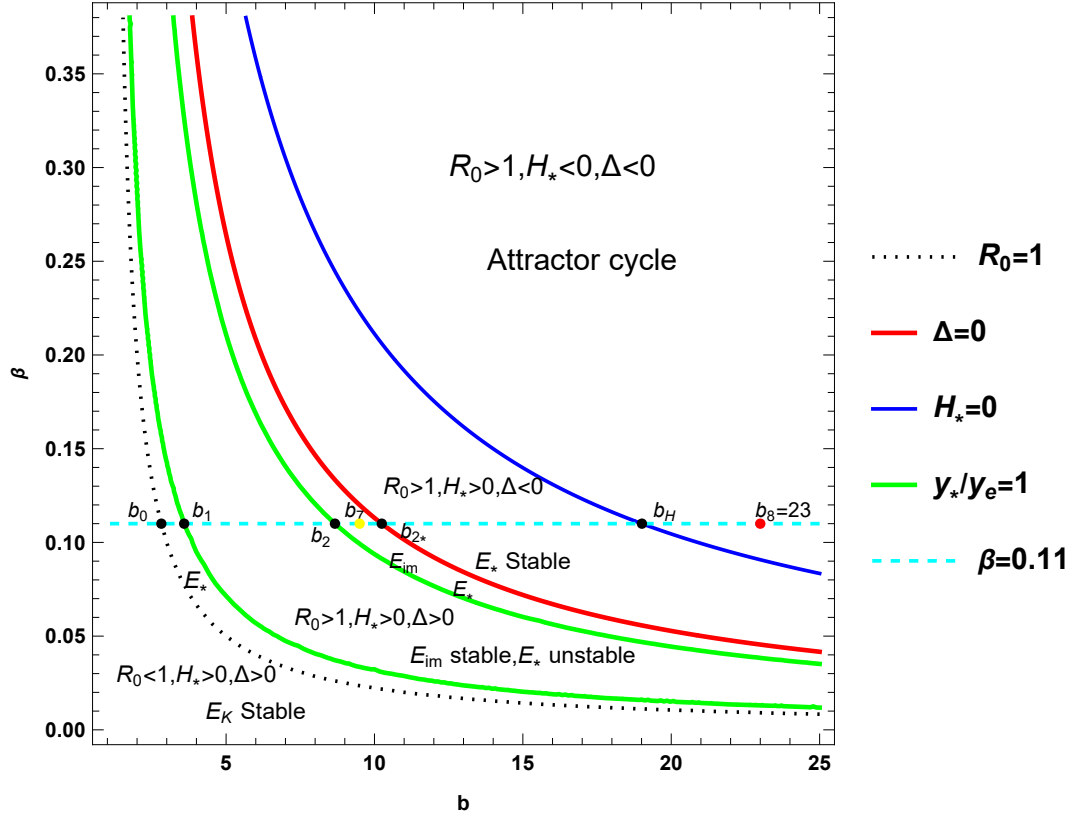


Figure 6: The partition of the  $(b, \beta)$  plane into six regions, when  $\beta_v = 0.16, \beta_y = 0.48, K = \gamma = 1, \Lambda = 0.36, \delta = 0.2, s = 0.6, c = 0.036$ . The region containing at least one attractor cycle is bounded below by the Hopf bifurcation curve  $H_*(b, \beta) = 0$ . Next follows a region where  $E_*$  is stable, bounded below by the curve  $\Delta(b, \beta) = 0$ , and then the bistability region  $b \in (b_2, b_{2*})$ , bounded below by the upper branch of  $\frac{y_*}{y_e} = 1$ . In between the two branches of  $\frac{y_*}{y_e} = 1$  we have a region where  $E_{im}$  is stable and  $E_*$  is unstable. Only  $E_*$  is stable in the next region, bounded below by the transcritical bifurcation curve  $R_0(b, \beta) = 1$ . In the last region,  $E_K$  is the only stable point. The phase plots at the points  $b_7$  and  $b_8$  are illustrated in Figures 7 and 8.

**Remark 4.3.** We conjecture, based on our numerical evidence, that it is impossible that  $E_{im}, E_+$  exchange stability, as suggested in [Phan and Tian, 2017, Prop. 8].

## 4.4 Time and phase plots illustrating bi-stability and a limit cycle, with $\epsilon = 0$

We provide now time and parametric plots illustrating these more “exotic” behaviours.

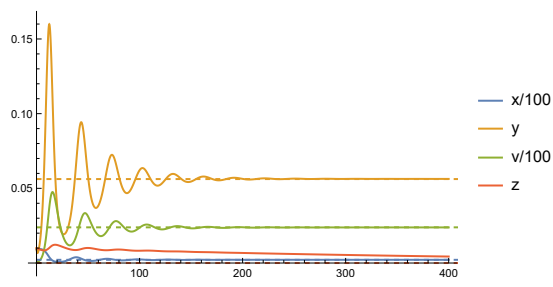
### 4.4.1 Bi-stability in the interval $(b_2, b_{2*})$

The parameters are fixed as in [Phan and Tian, 2017]:  $\beta_v = 0.16$ ,  $\beta_y = 0.48$ ,  $K = 1$ ,  $\gamma = 1$ ,  $\lambda = 0.36$ ,  $\beta = 0.11$ ,  $\delta = 0.2$ ,  $\beta_z = 0.6$ ,  $c = 0.036$ ,  $y_e = 0.06$ .

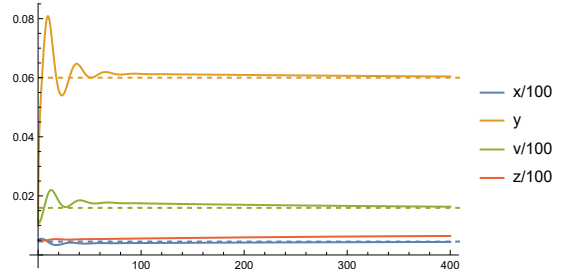
When  $b = 9.5 \in (b_2, b_{2*})$ ;

we obtain that  $E_* = (0.213904, 0.0562055, 2.38873, 0)$  and  $E_{im} = (0.453156, 0.06, 1.59331, 0.67437)$  with the eigenvalues  $(-1.25014, -0.0251954 \pm 0.21128Im, -0.0022767)$  and  $(-1.69595, -0.0714416 \pm 0.218669Im, -0.00574855)$ , respectively, are the unique stable attractors, as illustrated in Figure 7;

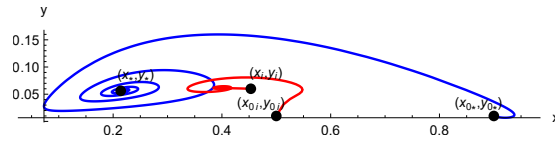




(a) Time plot of the four components indicates the convergence towards the attractor  $E_*$ .



(b) Time plot of the four components indicates the convergence towards the attractor  $E_{im}$ . with  $x_0 = z_0 = 0.5, y = 0.01$  and  $v_0 = 1.2$ .



(c)  $(x, y)$  parametric plots illustrating the convergence towards the fixed point  $E_{im}$  (in red) and towards  $E_*$  (in blue) with  $t_f = 1900$  and  $t_f = 200$ , respectively, when  $b = 10$  and  $(x_{0*}, y_{0*}) = (0.9, 0.01)$  and  $(x_{0i}, y_{0i}) = (0.5, 0.01)$ .

Figure 7: Plots of the evolution of the dynamics in time, and illustration of the convergence towards  $E_*$  and  $E_{im}$  when  $b = 9.5$ .

#### 4.4.2 Limit cycle in the interval $(b_H, b_\infty)$

When  $b = 23 > b_H$ , there is no stable attractor –see Figure 8;

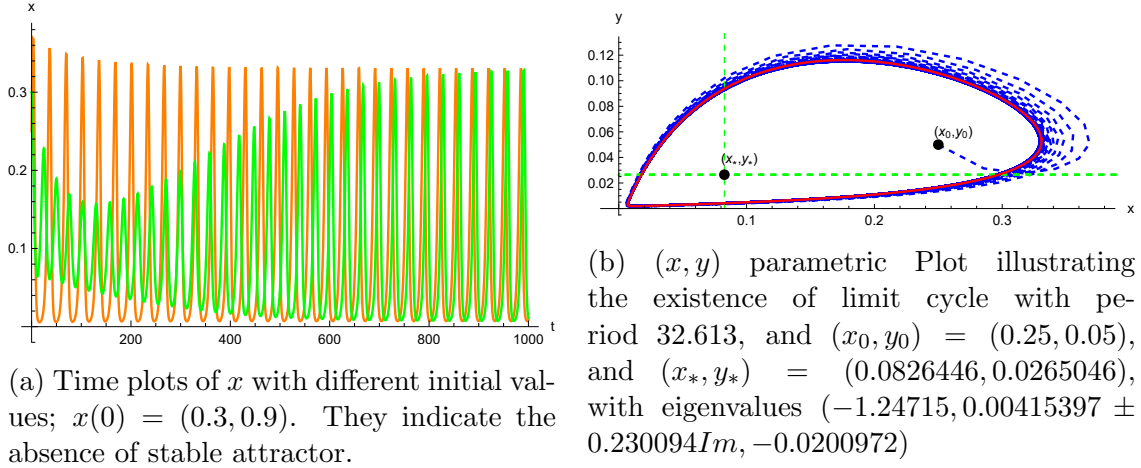


Figure 8:  $x$ -time plots and display of the parametric plots when  $b = 23$ .

## 5 The four-dimensional viro-therapy model of [Guo et al., 2019], with logistic growth

In this section, we turn to the special case of (1) when  $\epsilon = 1$ , that is,

$$\begin{aligned}
 \frac{dx}{dt} &= \lambda x \left( 1 - \frac{x+y}{K} \right) - \beta x v \\
 \frac{dy}{dt} &= \beta x v - \beta_y y z - \gamma y \\
 \frac{dv}{dt} &= b \gamma y - \beta x v - \beta_v v z - \delta v \\
 \frac{dz}{dt} &= z(sy - cz).
 \end{aligned} \tag{14}$$

### 5.1 Interior equilibria

**Theorem 5.1.** *A) There are at most three equilibrium points belonging to the interior of  $\mathbb{R}_+^4$ ;*

*B) Their  $y$  component is a zero of the third degree polynomial  $Q(y)$  defined in (17), and lies within*

$$\left( 0, y_b := \frac{c\gamma(b-1)}{\mu\beta_z} \right).$$

*Proof.* A) is immediate.

B) From the last equation in (1),  $z = y \frac{\beta_z}{c}$ . Adding the second and third equation in (1) yields

$$\gamma y(b-1) - \beta_y y z = v(\beta_v z + \delta),$$

we find that  $v = y \frac{f(y)}{g(y)}$ , where we put

$$\begin{cases} f(y) = c\gamma(b-1) - y\beta_y s \\ g(y) = \beta_v s y + \delta c. \end{cases} \quad (15)$$

From the second equation in (1)  $x = \frac{h(y)g(y)}{\beta f(y)}$ , where  $h(y) = y \frac{s\beta_y}{c} + \gamma$ , and  $xv = \frac{h(y)g(y)}{\beta f(y)} y \frac{f(y)}{g(y)} = y \frac{h(y)}{\beta}$ .

From (1),  $y$  must be a zero of the rational function

$$\lambda(1 - \frac{y}{K}) - \frac{\lambda}{K} \frac{h(y)g(y)}{\beta f(y)} - y \frac{\beta f(y)}{g(y)} := P(y) := \frac{Q(y)}{f(y)g(y)}, \quad (16)$$

and hence of its numerator, which is the third degree polynomial

$$Q(y) = \lambda f(y)g(y)(1 - \frac{y}{K}) - \frac{\lambda h(y)g(y)^2}{\beta K} - \beta y f(y)^2. \quad (17)$$

For  $x, v$  and  $z$  to be positive,  $y$  must lie in  $(0, y_b)$ .

□

The formulas for the coefficients of  $Q(y) = a_3 y^3 + a_2 y^2 + a_1 y + a_0$  are:

- $a_3 = (\frac{\beta_y \beta_z^2}{\beta K c})(\beta \beta_v c \lambda - \beta_v^2 s \lambda - K \beta^2 \beta_y c)$
- $a_2 = (\frac{\beta_z}{\beta K})(\beta \beta_y c r \delta + 2K \beta^2 \beta_y c \gamma(b-1) - \beta K \beta_v \beta_y s \lambda - \beta \beta_v c \gamma(b-1) \lambda - 2\beta_v \beta_y s \lambda \delta - \beta_v^2 s \gamma r)$
- $a_1 = (\frac{c}{K \beta})(\beta K \beta_v s \gamma(b-1) \lambda - \beta K \beta_y \lambda \delta - \beta c \gamma(b-1) \lambda \delta - \beta_y s \lambda \delta^2 - 2\beta_v s \gamma \lambda \delta - \beta^2 K c \gamma^2(b-1)^2)$
- $a_0 = \frac{\lambda c^2 \gamma \delta}{\beta K}(\beta K(b-1) - \delta).$

**Theorem 5.2.** *Suppose  $R_0 > 1$ . Then, there is at least one interior equilibrium point.*

1. *If furthermore  $a_3 > 0$  (large  $\beta$ ), then there is exactly only one interior equilibrium point.*

2. If  $a_3 < 0$  there can be 1, 2 or 3 interior equilibrium points, depending whether the discriminant is negative, zero, or positive. These interior points (when they exist) will be denoted by  $E_+$ ,  $E_-$ ,  $E_{im}$ , corresponding to the highest, lowest and intermediate values of  $y$ , respectively.

*Proof.* Observe that  $P(0) = \lambda(1 - \frac{\delta}{\beta K(b-1)})$  and  $P(0) > 0$  if and only if  $\delta < \beta K(b-1)$ , which holds from the assumption. And

$$\lim_{y \rightarrow y_b^-} P(y) = -\infty$$

Thus, by continuity,  $P(y)$  has at least one root  $y_0$  in  $(0, y_b)$ .

Alternatively, note that  $Q(y_b) = -\frac{\lambda h(y_b)g(y_b)^2}{\beta K} < 0$  (since  $g(y) > 0$  and  $h(y) > 0$  for all  $y > 0$ ), and that  $Q(0) = \frac{\lambda c^2 \gamma \delta}{\beta K} (\beta K(b-1) - \delta) > 0$  when  $R_0 > 1$ .

1. Recall that  $a_0 > 0$ . Descartes' rule of signs states that if there are  $k$  sign changes in the coefficients of a polynomial, ordered with exponent's decreasing order, then the number of positive real roots (counting multiplicities) equals to  $k$  or is less than this number by a positive even integer. If  $a_0 > 0$  and  $a_3 > 0$  then there can only be 0 or 2 changes of signs. Theorem 3.2 guarantees that there cannot be 0 changes, so there are 2 changes of signs. Now  $\lim_{y \rightarrow \infty} Q(y) = +\infty$  and  $Q(y_b) = -\frac{r\gamma b}{K\beta} g(y_b)^2 < 0$  imply that there is at least one root of  $Q(y)$  in  $(y_b, +\infty)$ . Thus there is only one root of  $P(y)$  in  $(0, y_b)$ , otherwise there would be at least 3 changes of signs and this cannot be possible.
2. If  $R_0 > 1$  and  $a_3 < 0$  there can only be 1 or 3 changes of signs. If there are 3 sign changes then there can be 1, 2 or 3 roots on the interval  $(0, y_b)$ . This case can only happen when  $a_1 < 0$ ,  $a_2 > 0$ ,  $a_3 < 0$ . Notice that  $a_1 \rightarrow -\infty$ ,  $a_2 \rightarrow +\infty$ ,  $a_3 \rightarrow -\infty$  as  $\beta \rightarrow +\infty$ , so the previous inequalities are indeed possible.

□

**Remark 5.1.** 1. If  $R_0 < 1$  there are no interior equilibrium points.

2. For the model of [Guo et al., 2019] with  $K = \infty$ ,  $Q(y)$  factors as the product of  $y - y_b$  and a second order polynomial.

## 5.2 Stability of interior equilibria and bifurcation diagrams

Now the Jacobian matrix evaluated on a interior equilibrium point  $E = (x, y, v, z)$  is given by

$$J(E) = \begin{pmatrix} \lambda - \frac{\lambda(2x+y)}{K} - v\beta & -\frac{\lambda x}{K} & -\beta x & 0 \\ \beta v & -\beta_y z - \gamma & \beta x & -\beta_y y \\ -\beta v & b\gamma & -\beta x - \beta_v z - \delta & -\beta_v y \\ 0 & \beta_z z & 0 & \beta_z y - 2cz \end{pmatrix}.$$

Its characteristic polynomial has a complicated form, its coefficients have been derived with the help of Mathematica, and the expression of the determinant is also long and complex, see the end of the first cell in [Mathematica, 2022c].

When the interior point  $E$  is either  $E_{im}$ ,  $E_+$  or  $E_-$ , the trace is given by

$$\begin{aligned} & -\frac{\lambda \left( \frac{2 \left( \frac{\beta_z y \beta_y}{c} + \gamma \right) (c\delta + sy\beta_v)}{\beta((b-1)c\gamma - sy\beta_y)} + y \right)}{K} + \frac{\beta_y (c(\gamma - b\gamma) + sy\beta_y)}{c\delta + sy\beta_v} - \frac{\left( \frac{\beta_z y \beta_y}{c} + \gamma \right) (c\delta + sy\beta_v)}{(b-1)c\gamma - sy\beta_y} \\ & - \frac{\beta_z y \beta_v}{c} - \frac{\beta_z y \beta_y}{c} - \gamma - \delta + \lambda - sy, \end{aligned}$$

and is negative for  $b \geq 1$ .

However, the check of the sum of the second and third order principal leading minors of the Jacobian at an interior equilibrium, the positivity of the determinant, and of the additional Hurwitz criterion, seemed to exceed our machine power, –see [Mathematica, 2022c, Subsection Ep1-2)].

We show in Figure 9 some bifurcation diagrams of the  $y$  component with respect to  $b$ ; for the corresponding stability analysis, see [Mathematica, 2022c, Subsection Ep1-3)].

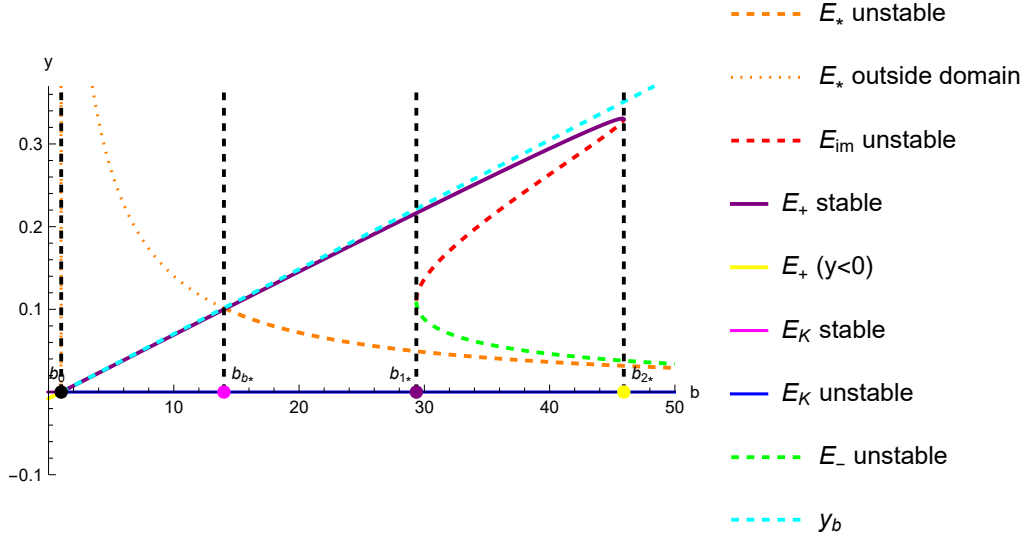


Figure 9: Bifurcation diagrams of the fixed points corresponding to the dynamics in (1), with respect to  $b$  and the coordinate  $y$  where  $y_* = \frac{\delta\lambda((b-1)\beta K - \delta)}{(b-1)\beta((b-1)\beta\gamma K + \delta\lambda)}$ , which is 0 when  $b = b_0 = 1.02299$ , as well as for  $E_+$ , with  $\epsilon = 1$  and  $K = 1$ . Here,  $\beta = \frac{87}{2}$ ,  $\lambda = 1$ ,  $\gamma = \frac{1}{128}$ ,  $\delta = 1/2$ ,  $\mu = 1$ ,  $\beta_v = 1$ ,  $\beta_z = 1$ ,  $c = 1$ , which yields the discriminant roots  $b_{1*} = 29.361$ ,  $b_{2*} = 45.9232$ , and the point of intersection of  $y_b$  and  $y_*$  is  $b_{b*} = 14.0011$ .

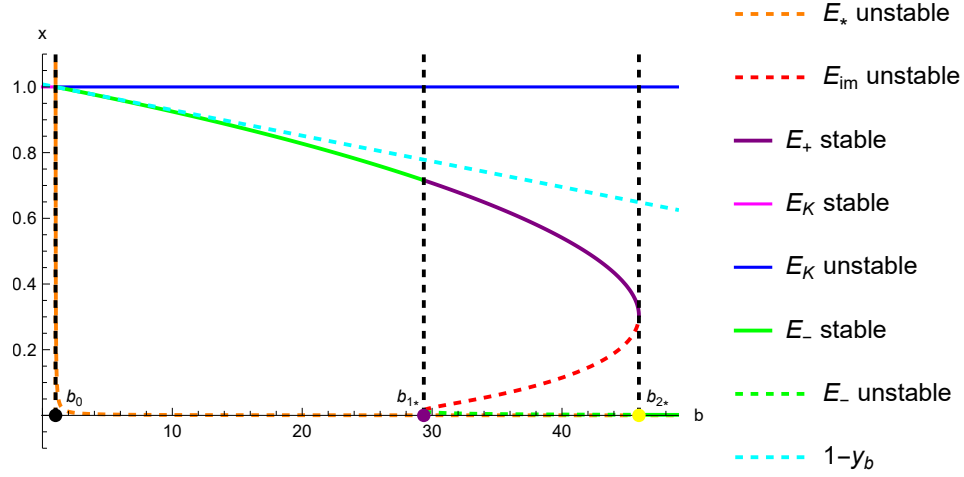


Figure 10: Bifurcation diagrams of the fixed points corresponding to the dynamics in (1), with respect to  $b$  and the coordinate  $x$  when  $\epsilon = 1$  and  $K = 1$ . Here,  $\beta = \frac{87}{2}$ ,  $\lambda = 1$ ,  $\gamma = \frac{1}{128}$ ,  $\delta = 1/2$ ,  $\mu = 1$ ,  $\beta_v = 1$ ,  $\beta_z = 1$ ,  $c = 1$ . When  $b > b_0$ ,  $x_*$  is very small, for example  $x_*(15) = 0.000821018$ . After  $b_{2*}$ ,  $x_*$  is very small, for example  $x_-(47) = 0.0017057$ .

With the parameters set as  $K = 1$ ,  $\beta = 87/2$ ,  $\lambda = 1$ ,  $\gamma = 1/128$ ,  $\delta = 1/2$ ,  $\beta_y = 1$ ,  $\beta_v = 1$ ,  $\beta_z = 1$ ,  $c = 1$  and taking  $b$  as the bifurcation parameter, we can use MatCont to verify that a Hopf bifurcation occurs at  $b_H = 29.903443$ . The corresponding first Lyapunov coefficient is 0.818234. The bifurcation diagram in Figure 11 reveals that there are two limit point cycles: one at  $b_{LC1} = 29.903500$  and one at  $b_{LC2} = 30.854713$ . A stable limit cycle bifurcates from the equilibrium  $E_{im}$  and exists for  $b > b_H$ . The MatCont code for the bifurcation analysis can be found at [Pérez, 2022].

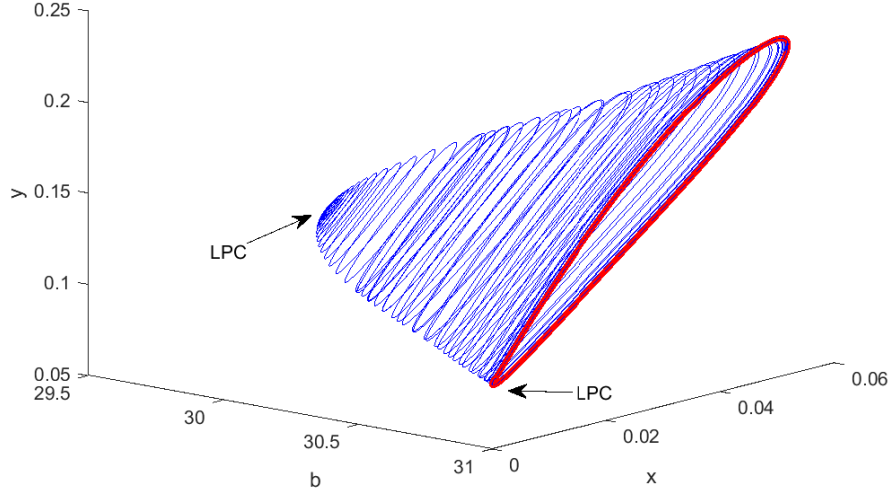


Figure 11: Bifurcation diagram for the dynamics of system (14) with respect to  $b$  and the  $(x, y)$  coordinates, showing the size of limit cycles as  $b$  varies. Two limit point cycles (labeled as LPC) are detected: one at  $b = 29.903500$  and one at  $b = 30.854713$ .

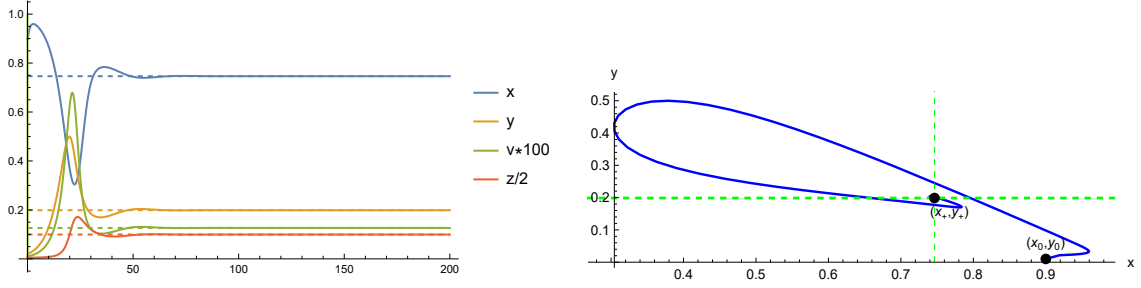
### 5.3 Time and phase plots illustrating different behaviors, with $\epsilon = 1$

In the following, we use the initial conditions  $x_0 = 0.9$ ,  $y_0 = v_0 = z_0 = 0.01$ , and the fixed parameters  $K = 1$ ,  $\beta = 87/2$ ,  $\lambda = 1$ ,  $\gamma = 1/128$ ,  $\delta = 1/2$ ,  $\beta_y = 1$ ,  $\beta_v = 1$ ,  $\beta_z = 1$ ,  $c = 1$  to illustrate via time plots of the four components and parametric plots the different dynamics of model (14) as  $b$  is varied.

#### 5.3.1 Stability of $E_+$ in the interval $(b_0, b_H)$

1. When  $b = 27 \in (b_0, b_{1*})$ , the unique stable attractor within the domain is  $E_+ = (0.746349, 0.198681, 0.001264, 0.198681)$  with eigenvalues  $(-33.4248, -0.6914, -0.1001 \pm 0.1725i)$ , and there are no other interior equilibria: see Figure 12 below.

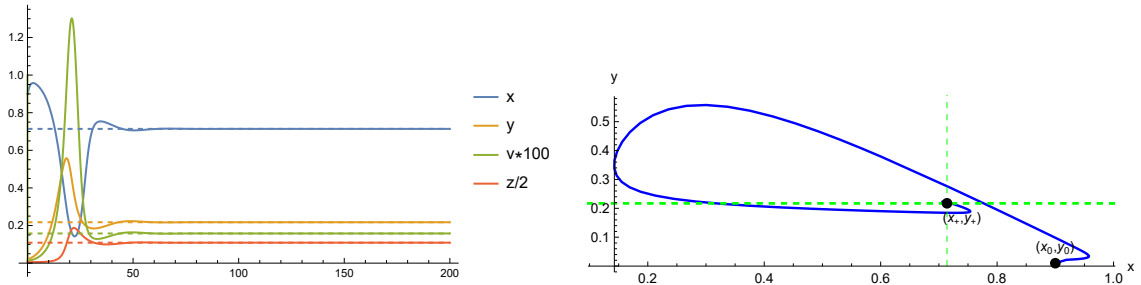




(a) Plot of the dynamics in time converging to the horizontal dashed lines, corresponding to the coordinates of the attractor  $E_+ = (0.746349, 0.198681, 0.001264, 0.198681)$ . (b)  $(x, y)$  parametric plot corresponding to  $E_+$  with  $t_f = 400$ .

Figure 12: Plots of the evolution of the dynamics in time, and a parametric plot corresponding to the attractor  $E_+$  when  $b = 27$ .

2. When  $b = 29.5 \in (b_{1*}, b_H)$ , there are three interior equilibria:  $E_+ = (0.713936, 0.217452, 0.001577, 0.217452)$ ,  $E_{im} = (0.018264, 0.121499, 0.019776, 0.121499)$  and  $E_- = (0.011907, 0.099053, 0.020438, 0.099053)$  with eigenvalues  $(-32.0654, -0.6453, -0.1098 \pm 0.1890i)$ ,  $(-1.9185, 0.1893, 0.0221 \pm 0.0654i)$  and  $(-1.5443, 0.1167 \pm 0.1115i, -0.0238)$ , respectively. The unique stable attractor is  $E_+$ , see Figure 13.



(a) Plot of the dynamics in time converging to the horizontal dashed lines, corresponding to the coordinates of the attractor  $E_+ = (0.713936, 0.217452, 0.001577, 0.217452)$ . (b)  $(x, y)$  parametric plot corresponding to  $E_+$  with  $t_f = 400$ .

Figure 13: Plots of the evolution of the dynamics in time, and a parametric plot corresponding to the attractor  $E_+$  when  $b = 29.5$ .

### 5.3.2 Bi-stability and limit cycle in the interval $(b_H, b_{2*})$

When  $b = 42 \in (b_H, b_{2*})$ , there exist three interior equilibria:  $E_+ = (0.494238, 0.308421, 0.004537, 0.308421)$ ,  $E_{im} = (0.145387, 0.284118, 0.0131148, 0.284118)$  and  $E_- = (0.002285, 0.042969, 0.021948, 0.042969)$  with eigenvalues  $(-22.81, -0.1575 \pm 0.2758i, -0.3016)$ ,  $(-7.8605, -0.1167 \pm 0.2540i, 0.2641)$  and  $(-0.8425, 0.0687 \pm 0.1676i, -0.0333)$ , respectively. In this case, there are two stable attractors: the equilibrium  $E_+$  and a stable limit cycle, see Figure 14.

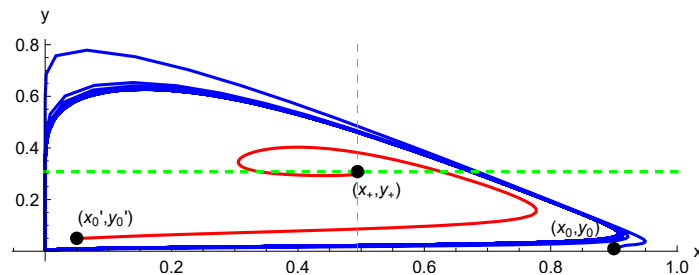


Figure 14: A two-dimensional phase space parametric picture of two trajectories, with initial values  $(x_0, y_0, v_0, z_0) = (0.9, 0.01, 0.01, 0.01)$  and  $(x'_0, y'_0, v'_0, z'_0) = (0.05, 0.05, 0.0043, 0.1954)$ , and the same value  $b = 42$ . The blue trajectory converges to a stable limit cycle, and the red trajectory converges to the interior equilibrium  $E_+$ .

### 5.3.3 Chaotic behavior in the interval $(b_{2*}, b_\infty)$

When  $b = 50 > b_{2*}$ , the only interior equilibrium is  $E_- = (0.001469, 0.033937, 0.022175, 0.033937)$  with eigenvalues  $(-0.7580, 0.0557 \pm 0.1632i, -0.0284)$ , and there is no stable attractor, see Figure 15.

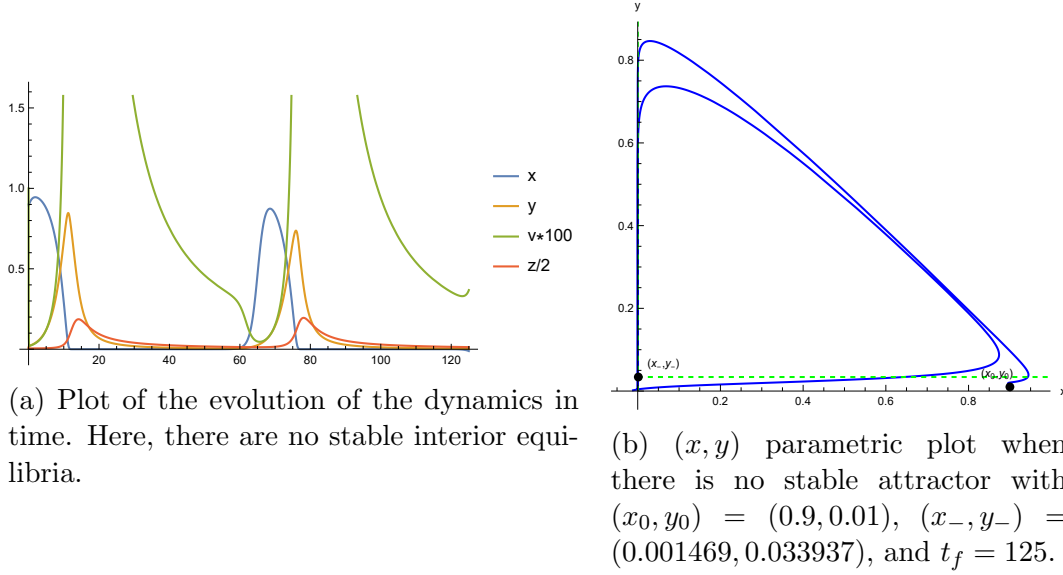


Figure 15: Plots of the evolution of the dynamics in time, and a parametric plot when  $b = 50$ .

## 6 Conclusions

In this study, we revisited the three-dimensional oncolytic virotherapy model of [Tian, 2011] and the four-dimensional model of [Phan and Tian, 2017], and we provided some new results obtained with the aid of Mathematica. Furthermore, we proposed a novel model with virotherapy and immunity that generalizes some of the previous works and established several results on the equilibrium points of this model. The use of electronic notebooks and software such as Mathematica and Matcont allowed us to illustrate the stability dynamics of the model and show the existence of stable limit cycles for certain sets of parameter values, which might pave the way for further research in this area.

## Acknowledgments

This article was supported in part by Mexican SNI under CVU 15284.

## References

- [Adenane, 2022] Adenane, R. (2022). GitHub repository. Four-dim-viro-therapy-M. <https://github.com/Rim-Adenane/Oncolytic-viro-therapy-models-M>.
- [Anderson and Jury, 1973] Anderson, B. and Jury, E. (1973). A simplified Schur-Cohn test. *IEEE Transactions on Automatic Control*, 18(2):157–163.
- [Anderson et al., 1989] Anderson, R. M., May, R. M., and Gupta, S. (1989). Non-linear phenomena in host–parasite interactions. *Parasitology*, 99(S1):S59–S79.
- [Antonio Chiocca, 2002] Antonio Chiocca, E. (2002). Oncolytic viruses. *Nature Reviews Cancer*, 2(12):938–950.
- [Blyth et al., 2020] Blyth, M., Renson, L., and Marucci, L. (2020). Tutorial of numerical continuation and bifurcation theory for systems and synthetic biology. *arXiv preprint arXiv:2008.05226*.
- [Bocharov et al., 2018] Bocharov, G., Volpert, V., Ludewig, B., Meyerhans, A., et al. (2018). *Mathematical immunology of virus infections*, volume 245. Springer.
- [Brown et al., 2006] Brown, C. W., Novotni, D., Weber, A., et al. (2006). Algorithmic methods for investigating equilibria in epidemic modeling. *Journal of Symbolic Computation*, 41(11):1157–1173.
- [Buckheit and Donoho, 1995] Buckheit, J. B. and Donoho, D. L. (1995). Wavelab and reproducible research. In *Wavelets and statistics*, pages 55–81. Springer.
- [Camara et al., 2022] Camara, B. I., Mokrani, H., Diouf, A., Sané, I., and Diallo, A. S. (2022). Stochastic model analysis of cancer oncolytic virus therapy: estimation of the extinction mean times and their probabilities. *Nonlinear Dynamics*, pages 1–28.
- [Chenar et al., 2018] Chenar, F. F., Kyrychko, Y. N., and Blyuss, K. B. (2018). Mathematical model of immune response to hepatitis B. *Journal of theoretical biology*, 447:98–110.
- [Claerbout and Karrenbach, 1992] Claerbout, J. F. and Karrenbach, M. (1992). Electronic documents give reproducible research a new meaning. In *SEG technical program expanded abstracts 1992*, pages 601–604. Society of Exploration Geophysicists.

- [Dalal et al., 2008] Dalal, N., Greenhalgh, D., and Mao, X. (2008). A stochastic model for internal HIV dynamics. *Journal of Mathematical Analysis and Applications*, 341(2):1084–1101.
- [Daud, 2021] Daud, A. A. M. (2021). A note on Lienard-Chipart criteria and its application to epidemic models. *Mathematics and Statistics*, 9(1):41–45.
- [Deng, 2001] Deng, B. (2001). Food chain chaos due to junction-fold point. *Chaos: An Interdisciplinary Journal of Nonlinear Science*, 11(3):514–525.
- [Deng, 2004] Deng, B. (2004). Food chain chaos with canard explosion. *Chaos: An Interdisciplinary Journal of Nonlinear Science*, 14(4):1083–1092.
- [Deng, 2006] Deng, B. (2006). Equilibriumizing all food chain chaos through reproductive efficiency. *Chaos: An Interdisciplinary Journal of Nonlinear Science*, 16(4):043125.
- [Deng et al., 2017] Deng, B., Han, M., and Hsu, S.-B. (2017). Numerical proof for chemostat chaos of shilnikov’s type. *Chaos: An Interdisciplinary Journal of Nonlinear Science*, 27(3):033106.
- [Deng and Hines, 2003] Deng, B. and Hines, G. (2003). Food chain chaos due to transcritical point. *Chaos: An Interdisciplinary Journal of Nonlinear Science*, 13(2):578–585.
- [Donoho, 2010] Donoho, D. L. (2010). An invitation to reproducible computational research. *Biostatistics*, 11(3):385–388.
- [Farkas and Simon, 1992] Farkas, H. and Simon, P. L. (1992). Use of the parametric representation method in revealing the root structure and Hopf bifurcation. *Journal of mathematical chemistry*, 9(4):323–339.
- [Friedman et al., 2006] Friedman, A., Tian, J. P., Fulci, G., Chiocca, E. A., and Wang, J. (2006). Glioma virotherapy: effects of innate immune suppression and increased viral replication capacity. *Cancer research*, 66(4):2314–2319.
- [Guckenheimer et al., 1997] Guckenheimer, J., Myers, M., and Sturmfels, B. (1997). Computing Hopf bifurcations I. *SIAM Journal on Numerical Analysis*, 34(1):1–21.
- [Guo et al., 2019] Guo, Y., Niu, B., and Tian, J. P. (2019). Backward Hopf bifurcation in a mathematical model for oncolytic virotherapy with the infection delay and innate immune effects. *Journal of biological dynamics*, 13(1):733–748.

- [Haddad et al., 2010] Haddad, W. M., Chellaboina, V., and Hui, Q. (2010). *Non-negative and compartmental dynamical systems*. Princeton University Press.
- [Hárs and Tóth, 1981] Hárs, V. and Tóth, J. (1981). On the inverse problem of reaction kinetics. *Qualitative theory of differential equations*, 30:363–379.
- [Huang et al., 2011] Huang, Z., Yang, Q., and Cao, J. (2011). Complex dynamics in a stochastic internal HIV model. *Chaos, Solitons & Fractals*, 44(11):954–963.
- [Kermack and McKendrick, 1927] Kermack, W. O. and McKendrick, A. G. (1927). A contribution to the mathematical theory of epidemics. *Proc. R. Soc. Lond. Series A, Containing papers of a mathematical and physical character*, 115(772):700–721.
- [Kim et al., 2020] Kim, D., Kim, H., Wu, H., and Shin, D.-H. (2020). The effect of the infection rate on oncolytic virotherapy. *Computational Biology and Bioinformatics*, 8(1).
- [Klebanoff and Hastings, 1994] Klebanoff, A. and Hastings, A. (1994). Chaos in three species food chains. *Journal of Mathematical Biology*, 32(5):427–451.
- [Kuznetsov et al., 2001] Kuznetsov, Y. A., De Feo, O., and Rinaldi, S. (2001). Belyakov homoclinic bifurcations in a tritrophic food chain model. *SIAM Journal on Applied Mathematics*, 62(2):462–487.
- [Kuznetsov and Rinaldi, 1996] Kuznetsov, Y. A. and Rinaldi, S. (1996). Remarks on food chain dynamics. *Mathematical biosciences*, 134(1):1–33.
- [Malkin, 1959] Malkin, I. G. (1959). *Theory of stability of motion*, volume 3352. US Atomic Energy Commission, Office of Technical Information.
- [Mathematica, 2022a] Mathematica (2022a). GitHub repository. Oncolytic-viro-therapy-models-M. <https://github.com/Rim-Adenane/Oncolytic-viro-therapy-models-M/blob/main/3dim-VF.nb>.
- [Mathematica, 2022b] Mathematica (2022b). GitHub repository. Oncolytic-viro-therapy-models-M. <https://github.com/Rim-Adenane/Oncolytic-viro-therapy-models-M/blob/main/4dim-ViroEp0.nb>.
- [Mathematica, 2022c] Mathematica (2022c). GitHub repository. Oncolytic-viro-therapy-models-M. <https://github.com/Rim-Adenane/Oncolytic-viro-therapy-models-M/blob/main/4dim-ViroEp1.nb>.

- [Nowak and May, 2000] Nowak, M. and May, R. M. (2000). *Virus dynamics: mathematical principles of immunology and virology: mathematical principles of immunology and virology*. Oxford University Press, UK.
- [O’Connell et al., 1999] O’Connell, J., Bennett, M. W., O’Sullivan, G. C., Collins, J. K., and Shanahan, F. (1999). The fas counterattack: cancer as a site of immune privilege. *Immunology today*, 20(1):46–52.
- [Perelson, 2002] Perelson, A. S. (2002). Modelling viral and immune system dynamics. *Nature reviews immunology*, 2(1):28–36.
- [Perelson and Nelson, 1999] Perelson, A. S. and Nelson, P. W. (1999). Mathematical analysis of HIV-1 dynamics in vivo. *SIAM review*, 41(1):3–44.
- [Perelson and Weisbuch, 1997] Perelson, A. S. and Weisbuch, G. (1997). Immunology for physicists. *Reviews of modern physics*, 69(4):1219.
- [Phan and Tian, 2017] Phan, T. A. and Tian, J. P. (2017). The role of the innate immune system in oncolytic virotherapy. *Computational and Mathematical Methods in Medicine*, 2017.
- [Phan and Tian, 2020] Phan, T. A. and Tian, J. P. (2020). Basic stochastic model for tumor virotherapy. *Mathematical Biosciences and Engineering*, 17(4):4271–4294.
- [Phan and Tian, 2022a] Phan, T. A. and Tian, J. P. (2022a). Hopf bifurcation without parameters in deterministic and stochastic modeling of cancer virotherapy, part i. *Journal of Mathematical Analysis and Applications*, 514(1):126278.
- [Phan and Tian, 2022b] Phan, T. A. and Tian, J. P. (2022b). Hopf bifurcation without parameters in deterministic and stochastic modeling of cancer virotherapy, part ii. *Journal of Mathematical Analysis and Applications*, 515(2):126444.
- [Pillis et al., 2006] Pillis, L. G., Gu, W., and Radunskaya, A. E. (2006). Mixed immunotherapy and chemotherapy of tumors: modeling, applications and biological interpretations. *Journal of theoretical biology*, 238(4):841–862.
- [Pooladvand, 2021] Pooladvand, P. (2021). *Mathematical Models in Oncolytic Virotherapy and Immunology*. PhD thesis, School of Mathematics and Statistics Faculty of Science, the University of Sydney, Australia.
- [Prodanov, 2021] Prodanov, E. M. (2021). Classification of the real roots of the quartic equation and their Pythagorean tunes. *International Journal of Applied and Computational Mathematics*, 7(6):1–14.

- [Pérez, 2022] Pérez, A. G. C. (2022). GitHub repository. Four-dimensional viro-therapy model. <https://github.com/agcp26/Four-dimensional-viro-therapy-model>.
- [Rockne et al., 2019] Rockne, R. C., Hawkins-Daarud, A., Swanson, K. R., Sluka, J. P., Glazier, J. A., Macklin, P., Hormuth, D. A., Jarrett, A. M., Lima, E. A., Oden, J. T., et al. (2019). The 2019 mathematical oncology roadmap. *Physical biology*, 16(4):041005.
- [Ruan and Wang, 2003] Ruan, S. and Wang, W. (2003). Dynamical behavior of an epidemic model with a nonlinear incidence rate. *Journal of differential equations*, 188(1):135–163.
- [Santiago et al., 2017] Santiago, D. N., Heidbuechel, J. P., Kandell, W. M., Walker, R., Djeu, J., Engeland, C. E., Abate-Daga, D., and Enderling, H. (2017). Fighting cancer with mathematics and viruses. *Viruses*, 9(9):239.
- [Senekal et al., 2021] Senekal, N. S., Mahasa, K. J., Eladdadi, A., de Pillis, L., and Ouifki, R. (2021). Natural killer cells recruitment in oncolytic virotherapy: A mathematical model. *Bulletin of Mathematical Biology*, 83(7):1–51.
- [Smith and De Leenheer, 2003] Smith, H. L. and De Leenheer, P. (2003). Virus dynamics: a global analysis. *SIAM Journal on Applied Mathematics*, 63(4):1313–1327.
- [Tian, 2011] Tian, J. P. (2011). The replicability of oncolytic virus: defining conditions in tumor virotherapy. *Mathematical Biosciences & Engineering*, 8(3):841.
- [Tóth et al., 2018] Tóth, J., Nagy, A. L., and Papp, D. (2018). *Reaction kinetics: exercises, programs and theorems*. Springer.
- [Tuckwell and Wan, 2000] Tuckwell, H. C. and Wan, F. Y. M. (2000). Nature of equilibria and effects of drug treatments in some simple viral population dynamical models. *Mathematical Medicine and Biology: A Journal of the IMA*, 17(4):311–327.
- [Van den Driessche and Watmough, 2002] Van den Driessche, P. and Watmough, J. (2002). Reproduction numbers and sub-threshold endemic equilibria for compartmental models of disease transmission. *Mathematical biosciences*, 180(1-2):29–48.



- [Van den Driessche and Watmough, 2008] Van den Driessche, P. and Watmough, J. (2008). Further notes on the basic reproduction number. In *Mathematical epidemiology*, pages 159–178. Springer.
- [Vithanage et al., 2021] Vithanage, G., Wei, H.-C., and Jang, S. R. (2021). Bistability in a model of tumor-immune system interactions with an oncolytic viral therapy. *apoptosis*, 1:7.
- [Wang et al., 2013] Wang, Y., Tian, J. P., and Wei, J. (2013). Lytic cycle: A defining process in oncolytic virotherapy. *Applied Mathematical Modelling*, 37(8):5962–5978.
- [Wiggers and Pedersen, 2018] Wiggers, S. L. and Pedersen, P. (2018). Routh–Hurwitz–Liénard–Chipart criteria. In *Structural stability and vibration*, pages 133–140. Springer.
- [Wodarz, 2003] Wodarz, D. (2003). Gene therapy for killing p53-negative cancer cells: use of replicating versus nonreplicating agents. *Human gene therapy*, 14(2):153–159.
- [Wodarz and Komarova, 2005] Wodarz, D. and Komarova, N. (2005). *Computational biology of cancer: lecture notes and mathematical modeling*. World Scientific.
- [Yu and Wei, 2009] Yu, C. and Wei, J. (2009). Stability and bifurcation analysis in a basic model of the immune response with delays. *Chaos, Solitons & Fractals*, 41(3):1223–1234.
- [Yuan and Allen, 2011] Yuan, Y. and Allen, L. J. S. (2011). Stochastic models for virus and immune system dynamics. *Mathematical biosciences*, 234(2):84–94.
- [Zenkov et al., 2002] Zenkov, D. V., Bloch, A. M., and Marsden, J. E. (2002). The Lyapunov–Malkin theorem and stabilization of the unicycle with rider. *Systems & control letters*, 45(4):293–302.